EDEM2 stably disulfide-bonded to TXNDC11 catalyzes the first mannose trimming step in mammalian glycoprotein ERAD

GINTO GEORGE

CONTENTS

ABSTRACT

Sequential mannose trimming of N-glycan ($Man_9GlcNAc_2$ -> $Man_8GlcNAc_2$ -> $Man_7GlcNAc_2$) facilitates endoplasmic reticulum-associated degradation of misfolded glycoproteins (gpERAD). Gene knockout experiments in human HCT116 cells have suggested that EDEM2 carries out the first step. However, it was previously shown that purified EDEM2 exhibited no α1,2 mannosidase activity toward $Man_9GlcNAc_2$ in vitro. Here, I found that EDEM2 was stably disulfide-bonded to TXNDC11, an endoplasmic reticulum protein containing five thioredoxin (Trx)-like domains. C558 present outside of the mannosidase homology domain of EDEM2 was linked to C692 in Trx5, which solely contains the CXXC motif in TXNDC11. This covalent bonding was essential for mannose trimming and subsequent gpERAD in HCT116 cells. TXNDC11 gene disruption leads to the loss of EDEM2 mannosidase activity and significant delay in gpERAD. EDEM2 showed altered protein conformation and increased degradation in the absence of its stable association with TXNDC11. Furthermore, EDEM2-TXNDC11 complex purified from transfected HCT116 cells converted $Man_9GlcNAc_2$ to $Man_8GlcNAc_2$ isomer B(M8B) in vitro. The present study establishes the role of EDEM2 as an initiator of gpERAD and represents the first clear demonstration of in vitro mannosidase activity of EDEM family proteins.

ABBREVIATIONS

AspN:	Endoproteinase Asp-N
CHX:	Cycloheximide
CNX:	Calnexin
CRT:	Calreticulin
DTT:	Dithiothreitol
EDEM:	ER degradation enhancing alpha mannosidase like protein
EndoH:	Endoglycosidase H
ER:	Endoplasmic Reticulum
ERAD:	ER-associated degradation
FDR:	False discovery rate
HCD:	Higher-energy collision dissociation
HPLC:	High-performance liquid chromatography
Htm1p:	Homologous to mannosidase I
MHD:	Mannosidase homology domain
Mns 1:	Alpha 1,2 mannosidase I
NEM:	N-Ethylmaleimide
ODS-column:	Octadecyl-silica- column
OS-9:	Osteosarcoma amplified 9
PA-M9:	Pyridylaminated M9
PITCh:	Precise Integration into Target Chromosome
PSM:	Peptide spectrum match
RT-PCR:	Reverse transcription polymerase chain reaction
TAP:	Tandem affinity purification
TCA:	Trichloroacetic acid

Tg:	Thapsigargin
TMD:	Transmembrane domain
Trx:	Thioredoxin
UGGT:	UDP-glucose: glycoprotein glucosyltransferase
Yos9:	Yeast homolog of OS 9

INTRODUCTION

Quality control (QC) is a critical step to ensure the proper assembly and specification in every manufacturing process. Pre-designed quality control screening is implied in every product human manufacture for humankind on planet earth. For every defective product we produce, we either try to repair it or, if that does not happen, discard it. Nature also follows the same system of sophisticated quality control screening to maintain the proper functioning of life processes. The cell, the basic building block of life, makes sure of its quality control in every step of DNA, RNA and protein synthesis.

In the case of proteins, quality control occurs during the steps of transcription, translation, folding and assembly. A protein must achieve its native conformation to surpass the final QC check points. In the endoplasmic reticulum (ER), misfolded proteins that cannot be brought back to their native state are recognized, ubiquitylated and targeted to the cytoplasm for proteasome degradation. These processes are collectively termed ER-associated degradation (ERAD) (Tsai et al., 2002).

In general, the ERAD pathway can be divided into four different steps: substrate recognition and targeting to the retro-translocation machinery; protein transport across the ER membrane and ubiqutilation; release of the substrate from the ER membrane into the cytosol; and degradation of the substrate (Fig 0.1) (Xie and Ng, 2010; Smith., et al 2011; Brodosky, 2012).

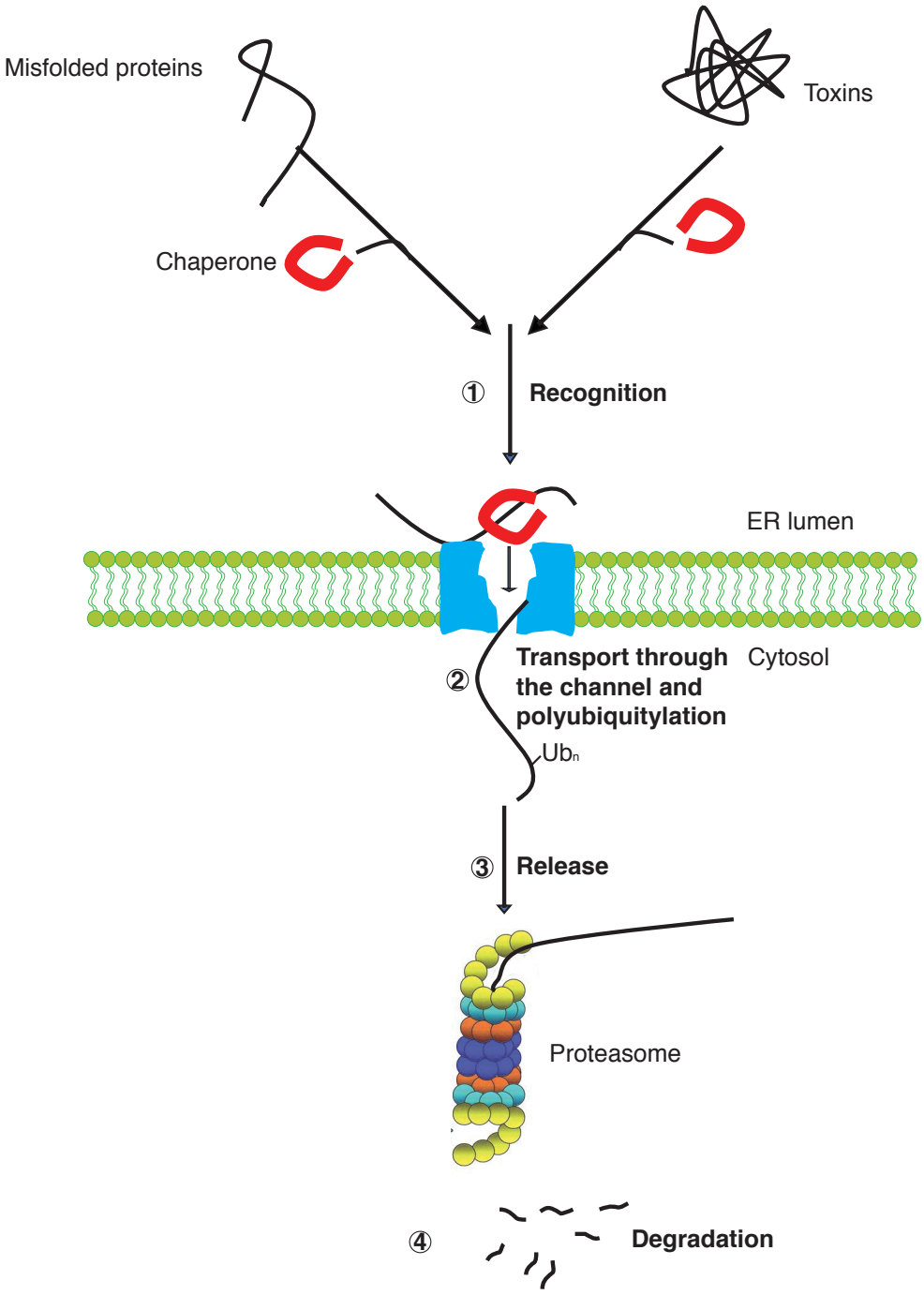

Fig. 0.1: Major steps of ERAD. In step 1, misfolded proteins are recognized and unfolded by ER chaperones and targeted to the translocon. Bacterial toxins probably adopt the same mechanism for unfolding. In step 2, polypeptides are moved through the channel. Polyubiquitylation (Ub_n) occurs when the polypeptide chain becomes exposed in the cytosol. In step 3, polyubiquitylated polypeptides are extracted from the ER membrane into the cytosol. In step 4, polypeptides are degraded by the proteasome (Tsai et al., 2002).

The ERAD pathway deals with different substates; hence, depending on the type of misfolded lesion, ERAD is classified into three pathways, ERAD-L (ERAD of substrates with misfolded lesions within the ER lumen), ERAD-C (cytoplasm), or ERAD-M (membrane) (Fig. 0.2) (Brodosky, 2012).

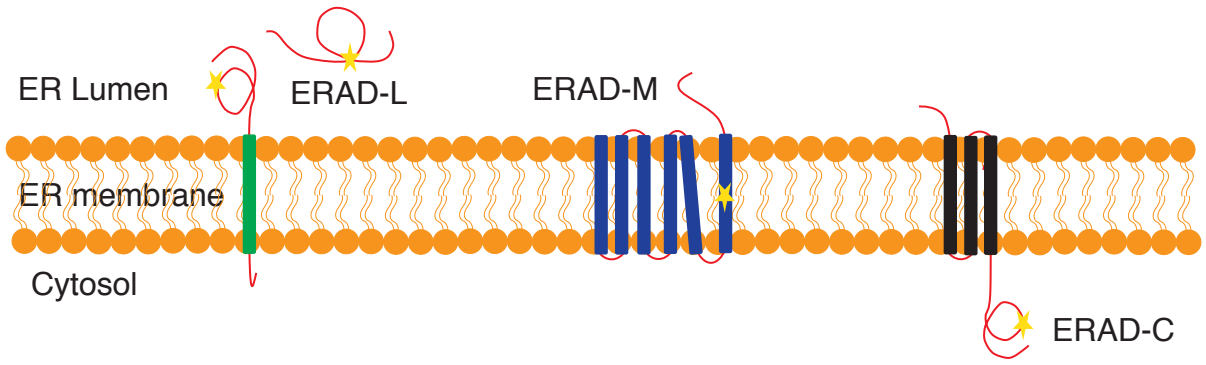

Fig 0.2: Major pathways of ERAD. ERAD-L: deals with substrates containing luminal folding lesions (yellow star). ERAD-M: deals with substrates containing a membrane-embedded folding lesion (yellow star). ERAD-C: deals with substrates containing cytosolic folding lesions (yellow star).

ERAD-L deals with the clearance of both glycosylated (gpERAD-L) and non-glycosylated (non-gpERAD-L) misfolded proteins from the lumen. The majority of nascent polypeptides that are translocated into the ER lumen are attached to the $Glc_3Man_9GlcNAc_2$ sugar moiety at an Asn residue, which is not only important for ensuring the proper topology but is also essential for their ERAD if they are unable to gain their native conformation. During the folding process of glycoproteins, the terminal three glucose residues are trimmed by glucosidase I and II sequentially to form $Man_9GlcNAc_2$ (Kamiya et al., 2012). In higher eukaryotes, the UDP-glucose glucosyltransferase (UGGT) repeatedly add glucose residues to $Man_9GlcNAc_2$. The mono-glucosylated glycoprotein is specifically recognized by two lectin chaperones, calnexin and calreticulin, and retained its localization in the ER until it gets folded (Fig 0.3). In gpERAD, the recognition of misfolded glycoproteins requires this N-linked glycan ($Man_9GlcNAc_2$) and protein determinant (Hammond et al., 1994; Ware et al., 1995; Hebert et al., 1995; Spiro et al., 1996).

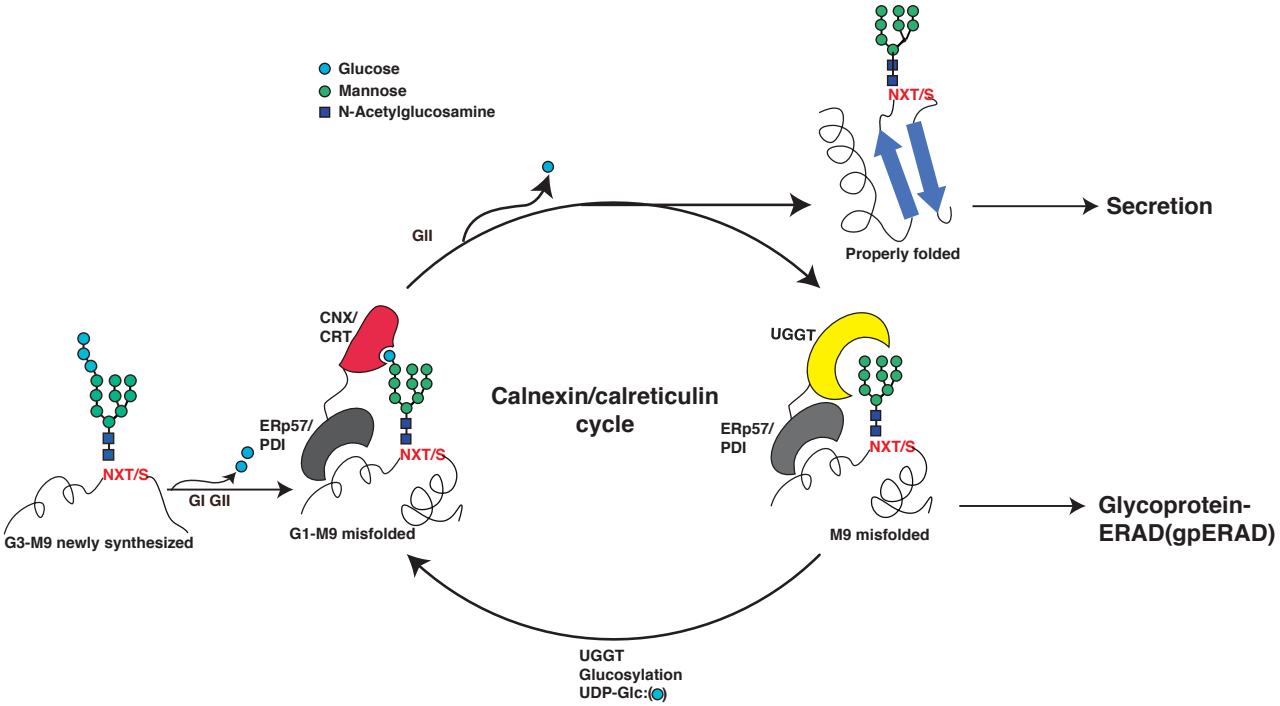

Fig 0.3: The calnexin/calreticulin cycle. Calnexin and calreticulin assist the folding of glycoproteins in the ER. Monoglucosylated ($Glc_1Man_9GlcNAc_2$) glycoprotein can interact with calnexin and calreticulin. Both chaperones associate with the thiol-disulfide oxidoreductase ERp57 or PDIs. Glucosidase II mediates cleavage of the remaining glucose which terminates the interaction with calnexin and calreticulin. Upon their release, correctly folded glycoproteins can exit the ER. On the other hand, non-native glycoproteins are substrates for the UDP-glucose: glycoprotein glucosyltransferase (UGGT), which adds a single glucose back onto the glycan and thereby promotes re-association with calnexin and calreticulin.

The recognition of misfolded glycoproteins in yeast gpERAD has been extensively studied. In this process, sequential mannose trimming from $Man_9GlcNAc_2$ to $Man_7GlcNAc_2$ plays a crucial role (Molinari, 2007; Hosokawa et al., 2010a; Kamiya et al., 2012). Briefly, in the first step, Mns1p, an α1,2-mannosidase, catalyzes the conversion of $Man_9GlcNAc_2$ (M9) to $Man_8GlcNAc_2$ isomer B (M8B); and α1,2-mannosidase Htm1p catalyzes the second step, conversion of M8B to $Man_7GlcNAc_2$ isomer A (M7A) with the α1,6-mannose exposed. M7A oligosaccharides are recognized by lectin Yos9p for subsequent retro-translocation to cytosol and degradation (Fig.0.4A) (Quan et al., 2008)

In mammalian ER, mannosidase I (ERmanI) is considered to be the sole homolog of Mns1. In contrast, Htm1p has 3 homologues, namely EDEM1, EDEM2, and EDEM3. The actual function of these proteins in mammalian gpERAD has remained elusive. According to the previous model, the mammalian gpERAD is initiated by ERmanI, which converts M9 to M8B (Gonzalez et al., 1999; Hosokawa et al., 2003). EDEM1 or EDEM3 then carry out the second step of M8B to M7 conversion (Hosokawa et al., 2003, 2010b; Hirao et al., 2006; Olivari et al., 2006). However, gene knockout studies of the mammalian homologues in chicken DT40 cells and human HCT116 cells indicated that EDEM2 initiates the gpERAD in mammals by trimming M9 to M8B and this M8B is further converted to M7A, primarily by EDEM3 and partly by EDEM1 (Ninagawa et al., 2014). M7A is further recognized by lectin proteins OS9 and XTP3B for retro-translocation to cytosol (van der Goot, 2018) (Fig 0.4 B).

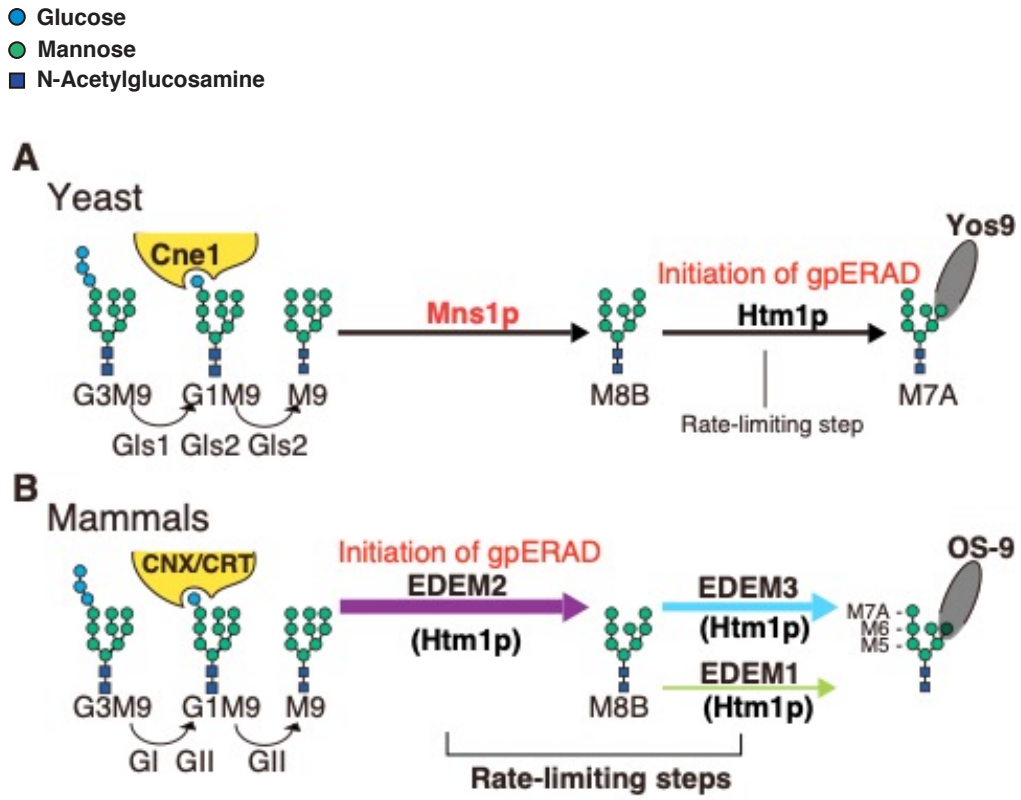

Fig 0.4: Current models of yeast and mammalian gpERAD. **(A)** In yeast, high-mannose-type oligosaccharide attached to asparagine ($Glc_3Man_9GlcNAc_2$, G3M9) is first trimmed to M9 by glucosidases Gls1 and Gls2. M9 is trimmed to M8B by Mns1p and M8B is trimmed to M7A by Htm1p. G1M9 is recognized by lectin chaperone Cne1p for folding, whereas M7A exposing α1,6-mannose is recognized by lectin Yos9p for subsequent degradation. **(B)** In mammals, G3M9 is trimmed to M9 by glucosidase I (GI) and glucosidase II (GII), homologues of yeast Gls1 and Gls2, respectively. G1M9 is recognized by lectin chaperones calnexin (CNX) and calreticulin (CRT), homologues of yeast Cne1p, for folding. In two rate-limiting steps of the mammalian gpERAD, M9 is trimmed to M8B by EDEM2, and M8B is trimmed by EDEM1 and EDEM3 to $Man_{7-5}GlcNAc_2$, which is recognized by lectin proteins OS-9 and XTP3B, homologues of yeast Yos9, for degradation (Ninagawa et al., 2014).

However, the confirmation of these homologues as true mannosidases can be achieved by checking their mannosidase activity in vitro. It was previously reported that recombinant EDEM2 purified from HEK293 cells showed no mannosidase activity towards pyridylamine (PA)-tagged $Man_9GlcNAc_2$ or PA-tagged $Man_8GlcNAc_2$ in vitro (Mast et al., 2005). Hence, the mannosidase activity of EDEM2 remains in debate.

Interestingly, studies on the mannosidase activity of Htm1p revealed the role of PDI-like proteins in its mannosidase activity. Htm1p is stably disulfide-bonded to Pdi1p, a protein disulfide isomerase, via the C-terminal domain (Clerc et al., 2009; Sakoh-Nakatogawa et al., 2009). The association of Pdi1p leads to introduction of a disulfide bond between C65 and C445 in the Mannosidase Homology Domain (MHD) for its mannosidase function (Sakoh-Nakatogawa et al., 2009). The Htm1p-Pdi1p complex was able to convert M8B to M7 in vitro (Gauss et al., 2011). Recently, Yu et al. showed the importance of an oxidoreductase, ERp46, on EDEM3 mannosidase activity (Yu et al., 2018). In this regard, it is possible that EDEM2 also requires a PDI-like partner protein to function as an active mannosidase.

Recent genome-wide CRISPR/Cas9-mediated forward genetic screening in human cells showed the importance of a type II transmembrane protein containing thioredoxin (TXNDC11) for gpERAD (Timms et al., 2016). It was shown that TXNDC11 exhibits the reductase activity required for the degradation of various gpERAD substrates, such as CD3δ, TCRα and NHK (null Hong Kong variant of α1-proteinase inhibitor), but not for degradation of non-gpERAD substrates. Mass spectroscopic analysis revealed that TXNDC11 can interact with the EDEM proteins EDEM2 and EDEM3 (Timms et al., 2016).

RESULTS

Sequence analysis between EDEM2 and Htm1p

I checked the sequence similarity between EDEM2 and its yeast homologue Htm1p with particular regard to the cysteine residues. The analysis revealed that the important cysteines of the MHD domain (C65 and C445) in Htm1p were strictly conserved in EDEM2 (C65 and C408) (Fig.1A, shown with black bars). Additionally, the C-terminal cysteine in Htm1p (C579), which was found to be important for the stable association with Pdi1p (Sakoh-Nakatogawa et al., 2009), was also conserved in EDEM2 (C558) (Fig. 1A, shown in red color and Fig. 1B). Sequence comparison showed that the conserved cysteine residues in the MHD domain are a common feature in all EDEMs (Fig. 1C).

A

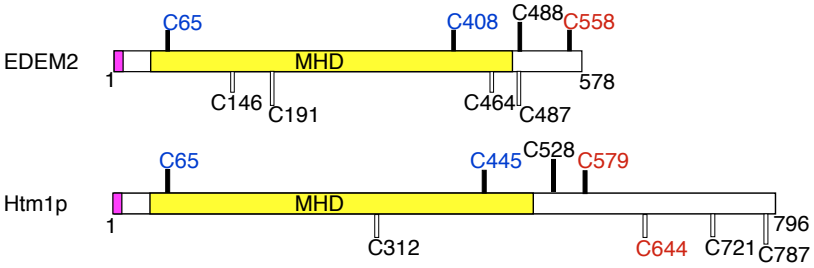

B

```
          65
EDEM2  DELRPLTCDG-------------HDTWGSFSLTLIDALDTLLILGNVSEFQRVVEVLQ-- 102
Htm1p  DEVKPISCVPKKRNFEDPTDQGTNDILGNFTITLIDSLTTIAILEDRPQFLKAVRLVERT 117
       **::*::*                :*  *.*::****:* *: ** :  :* :.*.:::
                                  408
EDEM2  LYRATGDPTLLELGRDAVESIEKISKVECGFATIKDLRDHKLDNRMESFFLAETVKYLYL 439
Htm1p  LYRATKDPFYLNIGVHLLKDLKQRFKSNCGFAGFQNVITGELQDRMETFVLSETLKYLYL 476
       ***** **  *::* . ::.:::  * :**** ::::   :*::***:*.*:**:*****

          488
EDEM2  --PAALHCCQRLKEEQWEVEDLMREFYSLKRSRSKFQKNTVSSGPWEPPAR-PGTLFSPE 538
Htm1p  VYSSHLEICQKKDREQAGENTLSQRIV-------GFAKSIFHKGPPDEEATDPIIDYTID 572
          : *. **: ..**   : * :.:         * *. . .** :  *  *   :: :

                   558
EDEM2  NHDQARERKPAKQKVPLLSCPSQPFTSKLALLGQVFLDSS-------------------- 578
Htm1p  ------TELP-------GTCSIKPH----HVIGDEFWYSPMLSNFDRLFEIDSRFAATLI 615
             . *        :*  :*.     ::*: *  *
```

C

```
                                                  65
EDEM1  ---AFPPQLRAQMRDLARGMFVFGYDNYMAHAFPQDELNPIHCRGRGPDRGDPSNLNIND 177
EDEM2  --------DPAHYRERVKAMFYHAYDSYLENAFPFDELRPLTCDGH-------------D 69
EDEM3  GAEPMSREEKQKLGNQVLEMFDHAYGNYMEHAYPADELMPLTCRGRVRG-QEPSRGDVDD 98
                  :  : .  ** ..*..*: :*:* *** *: * *:              *
                                                                  408
EDEM1  LPERYNWQLQ--APDVLFYPLRPELVESTYLLYQATKNPFYLHVGMDILQSLEKYTKVKC 529
EDEM2  LPEFYNIPQGYTVEKREGYPLRPELIESAMYLYRATGDPTLLELGRDAVESIEKISKVEC 408
EDEM3  LPEAFTTDFRV---HWAQHPLRPEFAESTYFLYKATGDPYYLEVGKTLIENLNKYARVPC 441
       *** :.        .   :*****: **:  **:** :*  *.:*   ::.::* ::* *

EDEM1  KSIYMRQIDQMVGLI---------------------------------------------- 657
EDEM2  LSCPSQPFTSKLALLGQ---------------------------------------------- 572
EDEM3  IHL----KDGRVQLVQHAIQAASSIDAEDGLRFMQEMIELSSQQQKEQQLPPRAVQIVSH 655
                  : *:
```

Figure 1: Sequence comparison between EDEM2 and Htm1p

(A) Structures of human EDEM2 and yeast Htm1p are schematically shown with cysteine residues (C) highlighted together with their positions (black bars underneath C indicate conserved cysteine residues, whereas white bars over C indicate non-conserved cysteine residues). The red and yellow boxes denote the signal sequence and mannosidase homology domain (MHD), respectively. **(B)** Sequence comparison around the four cysteine residues conserved between EDEM2 and Htm1p (marked in red color) is shown below (asterisk and colon indicate identical and similar amino acid, respectively). **(C)** Sequence comparison between the EDEM homologues EDEM1, EDEM2 and EDEM3. The conserved cysteines between the homologues are highlighted in red (asterisk and colon indicate identical and similar amino acid, respectively.

Evaluation of cysteine residues present in EDEM2 for its mannosidase activity.

I intended to check the role of cysteines present in EDEM2 for its mannosidase activity. EDEM2 has eight cysteine residues, of which five are located in the MHD domain and the remaining three are in the C-terminal region. By using mutated primers, I mutated each cysteine of EDEM2 to an alanine and checked their activity of mannose trimming from ERAD-L substrate mCD3-δ-ΔTM-HA, which has three N-glycosylation sites. In the absence of EDEM2 (EDEM2-KO), mCD3-δ-ΔTM-HA showed slower migration due to the inability of the first mannose trimming. The migration difference disappeared after removal of N-glycans by treatment with endoglycosidase (EndoH) (Fig. 2A). Co-expression of Flag-tagged EDEM2 WT and each cysteine mutant with mCD3-δ-ΔTM-HA in EDEM2-KO cells recovered mannose trimming defect, except in the case of three cysteine mutants, namely C65A, C408A and C558A. I used a catalytic-inactive mutant, E117Q as control (Fig. 2B). Degradation assay using cycloheximide chase clearly showed that mCD3-δ-ΔTM-HA degradation is significantly delayed in the trimming defective cysteine mutants, similar to the case with EDEM2-KO cells (Fig. 2C).

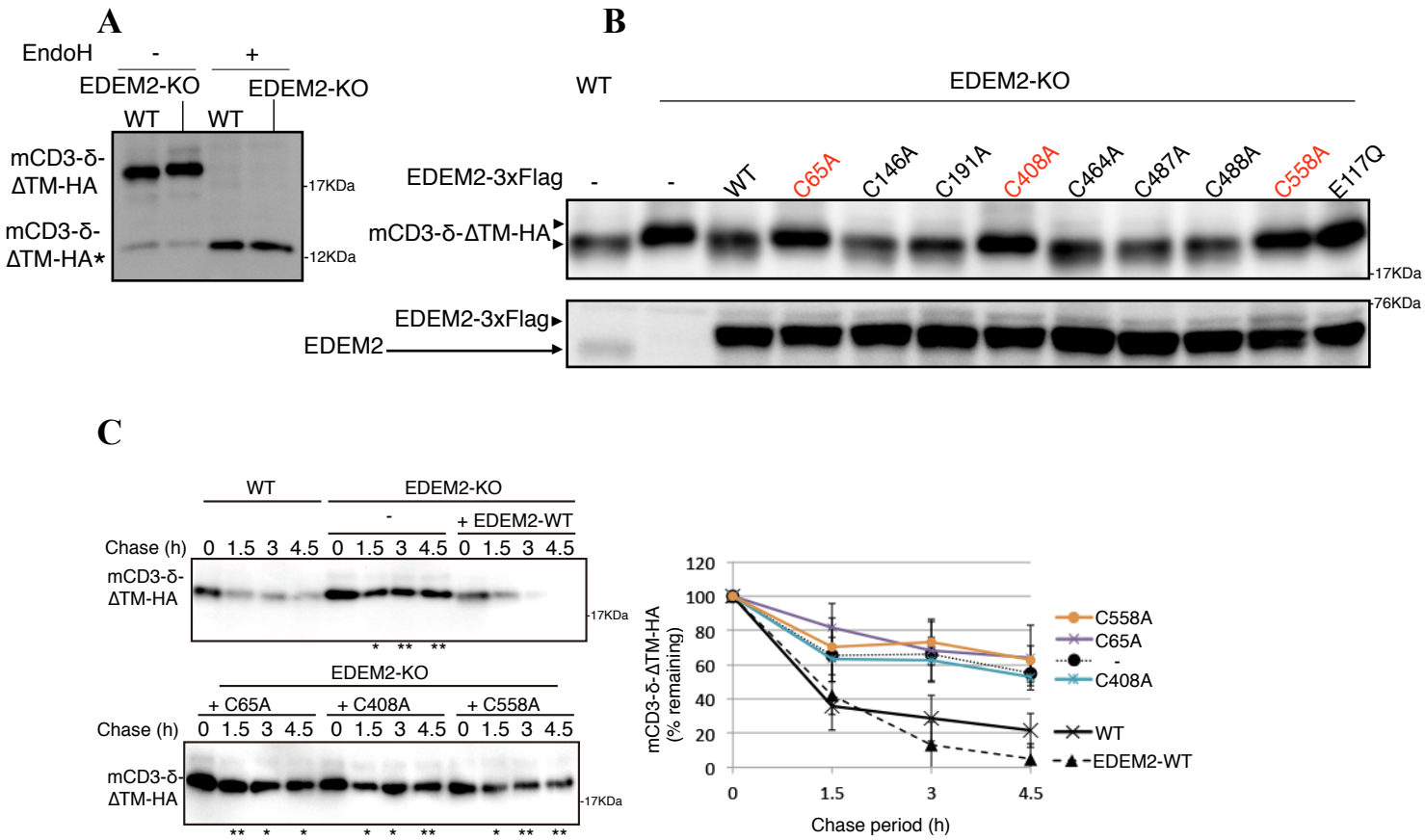

Figure 2: Requirement of cysteine residues present in EDEM2 for its mannosidase activity.

(A) Cell lysates were prepared from WT and EDEM2-KO cells expressing mCD3-δ-ΔTM-HA by transfection, treated with (+) or without (-) EndoH, and analyzed by immunoblotting using anti-HA antibody. mCD3-δ-ΔTM-HA* denotes deglycosylated mCD3-δ-ΔTM-HA. **(B)** Cell lysates were prepared from WT and EDEM2-KO cells expressing WT or one of the various cysteine mutants of 3x Flag-tagged EDEM2 together with mCD3-δ-ΔTM-HA by transfection, and analyzed by immunoblotting using anti-HA and anti-EDEM2 antibodies. E117Q is an enzymatically inactive mutant of EDEM2. **(C)** Cycloheximide chase was conducted to determine the degradation rate of mCD3-δ-ΔTM-HA in WT and EDEM2-KO cells expressing WT or one of the three cysteine mutants of 3x Flag-tagged EDEM2 by transfection, and analyzed by immunoblotting using anti-HA antibody (n=3). Quantified data are shown on the right. *P<0.05, **P<0.01.

Interaction of EDEM2 with thioredoxin family proteins.

I checked the interaction of EDEM2 with its partners, especially thioredoxin-containing proteins. I performed an immunoprecipitation (IP) experiment using transiently expressed EDEM2(WT)-3xFlag, EDEM2(C65A)-3xFlag, EDEM2(C408A)-3xFlag, and EDEM2(C558A)-3xFlag in EDEM2-KO cells and subjected the immunoprecipitates to immunobloting with anti-PDI, anti-TXNDC11, or anti-ERp72 antibodies. I found that both PDI and TXNDC11 interacted with EDEM2. In addition, the C558A mutation disrupted the binding of EDEM2 with TXNDC11, whereas PDI interaction was unaffected by the mutation (Fig. 3A, reducing). I noticed that in the non-reducing gel, the immunoprecipitates reacted with anti-TXNDC11antibody in a higher molecular weight band (~225KDa) in the WT, C65A, and C408A versions of EDEM2 protein but not in the case of C558A mutants (Fig. 3A, non-reducing). The higher molecular weight band of C65A, and C408A mutants in non-reducing SDS-PAGE in the IP experiment showed a difference in migration compared to the WT (Fig. 3A, non-reducing). To check whether this difference in migration was due to the defect in N-glycan trimming, I conducted the same experiment using WT cells. The results still showed the difference in migration between WT and C65A and C408A versions of the protein, indicating that it is due to the change in the conformation of the complex due to cysteine mutation (Fig. 3B, non-reducing).

Interestingly, both a monomer and higher molecular weight band were detected in non-reducing SDS-PAGE, which specifically reacts with anti-TXNDC11 antibody but not with anti-PDI antibody (Fig. 3C). Together, these results indicate that EDEM2 stably interacts with TXNDC11 via disulfide bond formation through the C558 cysteine residue.

A

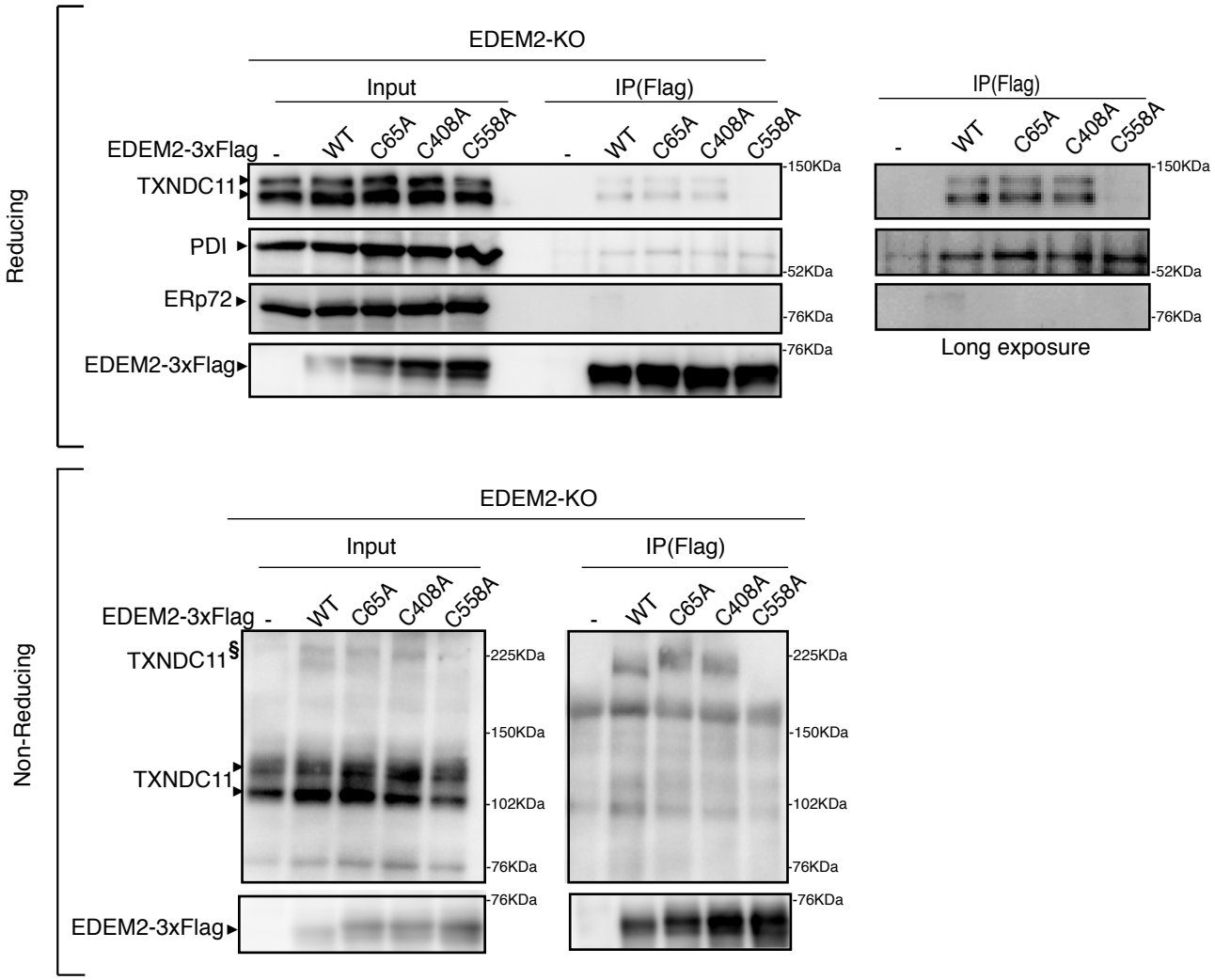

Figure 3: Interaction of EDEM2 with thioredoxin family proteins

(A) Cell lysates were prepared from EDEM2-KO cells expressing WT or one of the three cysteine mutants of 3xFlag-tagged EDEM2 by transfection and subjected to immunoprecipitation using anti-Flag antibody. Aliquots of cell lysates (Input) and immunoprecipitates {IP(Flag)} were subjected to SDS-PAGE under reducing and non-reducing conditions, and analyzed by immunoblotting using anti-TXNDC11, anti-PDI, anti-ERp72, and anti-Flag antibodies.

B

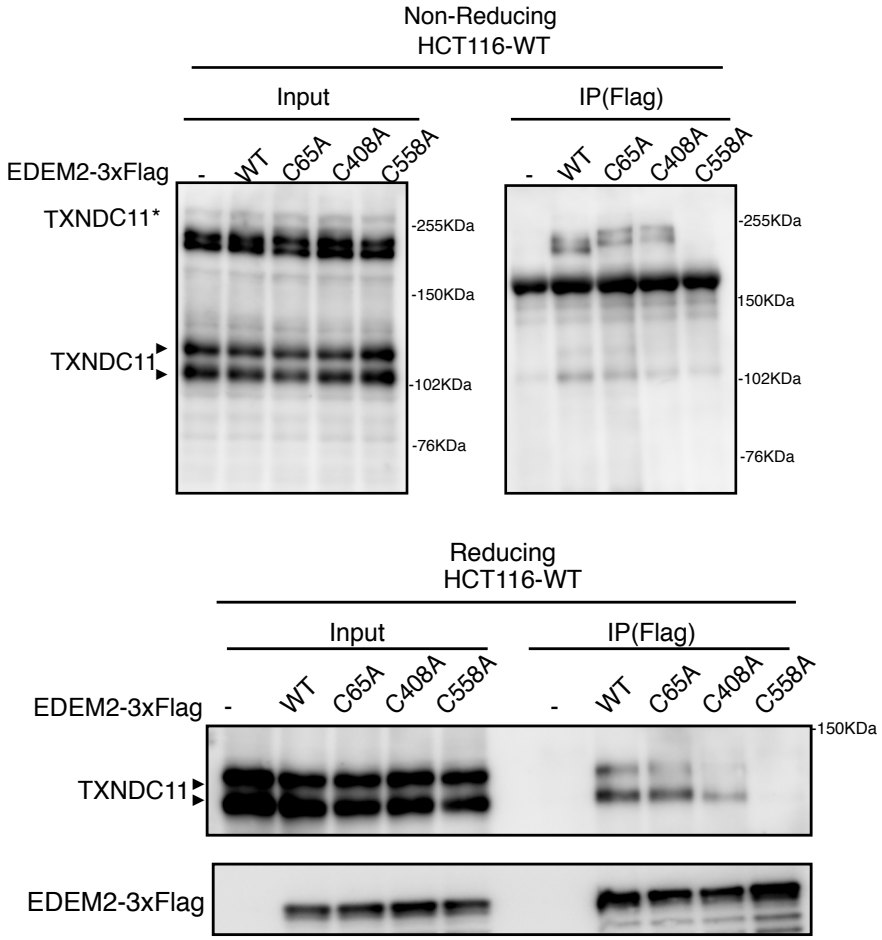

Figure 3 continued.

(B) Cell lysates were prepared from HCT116 WT cells expressing WT or one of the three cysteine mutants of 3xFlag-tagged EDEM2 by transfection and subjected to immunoprecipitation using anti-Flag antibody. Aliquots of cell lysates (Input) and immunoprecipitates {IP(Flag)} were subjected to SDS-PAGE under reducing and non-reducing conditions, and analyzed by immunoblotting using anti-TXNDC11 and anti-Flag antibodies.

C

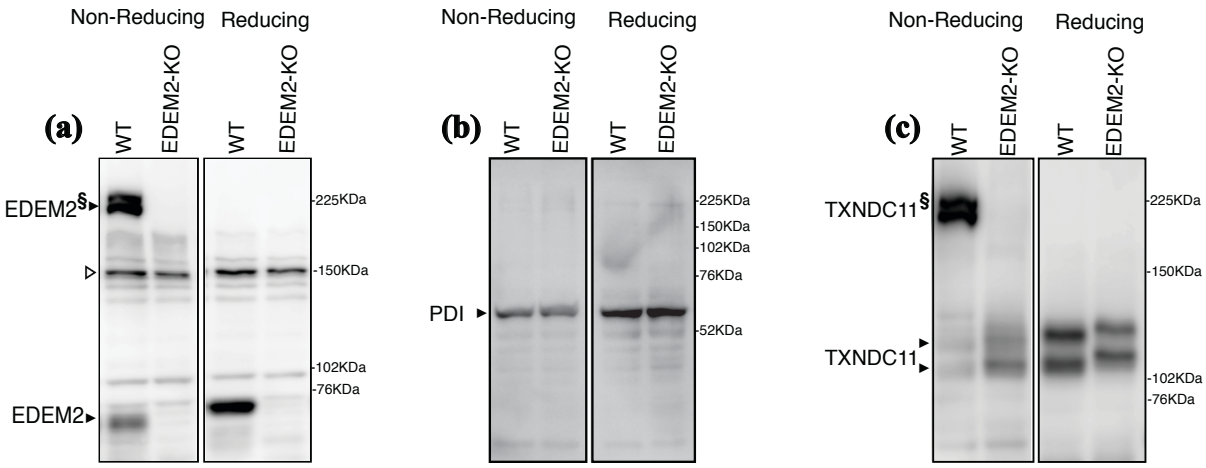

Figure 3 continued.

(C) Cell lysates were prepared from WT and EDEM2-KO cells, subjected to SDS-PAGE under reducing and non-reducing conditions, and analyzed by immunoblotting using anti-EDEM2 (a), anti-PDI (b) and anti-TXNDC11 (c) antibodies. § denotes high molecular weight forms of EDEM2 and TXNDC11. Open triangle indicates a non-specific band.

Construction of TXNDC11-KO in HCT116 cell line

As C558A mutation in EDEM2 leads to its loss of interaction with TXNDC11, and loss of mannosidase activity, I thought that TXNDC11 might play some important role in maintaining the mannosidase activity of EDEM2. To evaluate this, I disrupted the *TXNDC11* gene in HCT116 cells using CRISPR/Cas9-based Precise Integration into Target Chromosome (PITCh). I targeted the exon one region of the gene with puromycin-resistant gene flanked by the left and right arms of *TXNDC11* gene as well as guide RNA target sites (Fig. 4A).

After co-transfection with both targeting vector and gRNA vector, I screened 34 colonies which showed puromycin resistance and chose two independent clones having insertion of puromycin-resistant gene at the target site (Fig. 4D). However, sequencing analysis of the inserted region from the genomic PCR products showed that Cas9 cleaved the targeting vector on only one side (upstream of the left arm in the case of KO#1 or downstream of the right arm in the case of KO#2); therefore, the whole targeting plasmid vector was integrated into the exon one region in one allele of both clones (Fig. 4B and C). The results also indicated that partial fragments of the targeting vector were inserted into exon one in another allele (Fig. 4B and C). Nevertheless, the inserts disrupted the expression of TXNDC11 at both mRNA and protein levels (Fig. 4E and F).

A

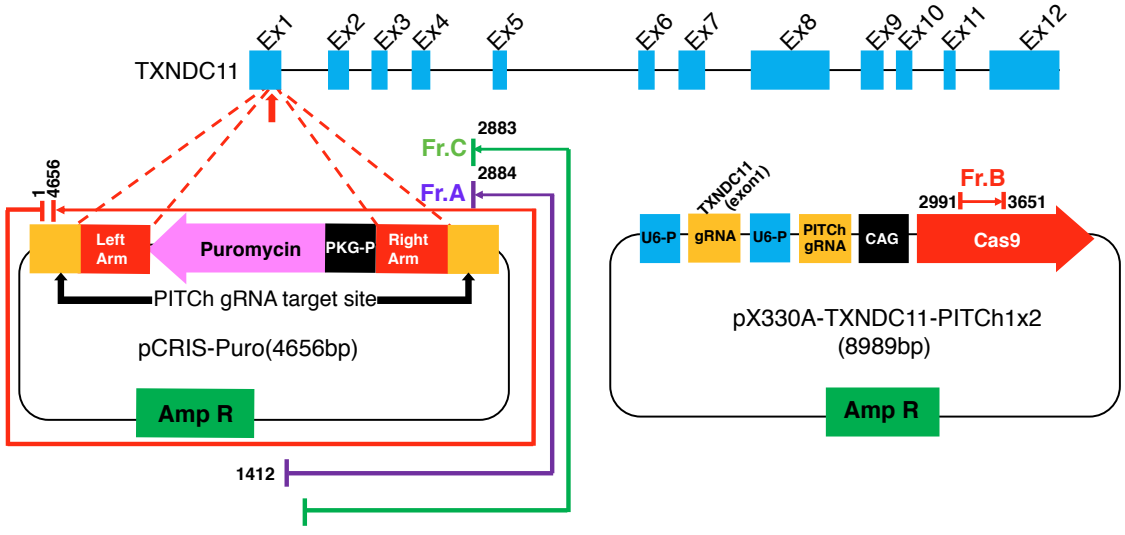

Figure 4: Construction of TXNDC11-KO in HCT116 cell line

(A) Strategy of the CRISPR/Cas9-based PITCh method to target exon 1 of the *TXNDC11* gene is shown.

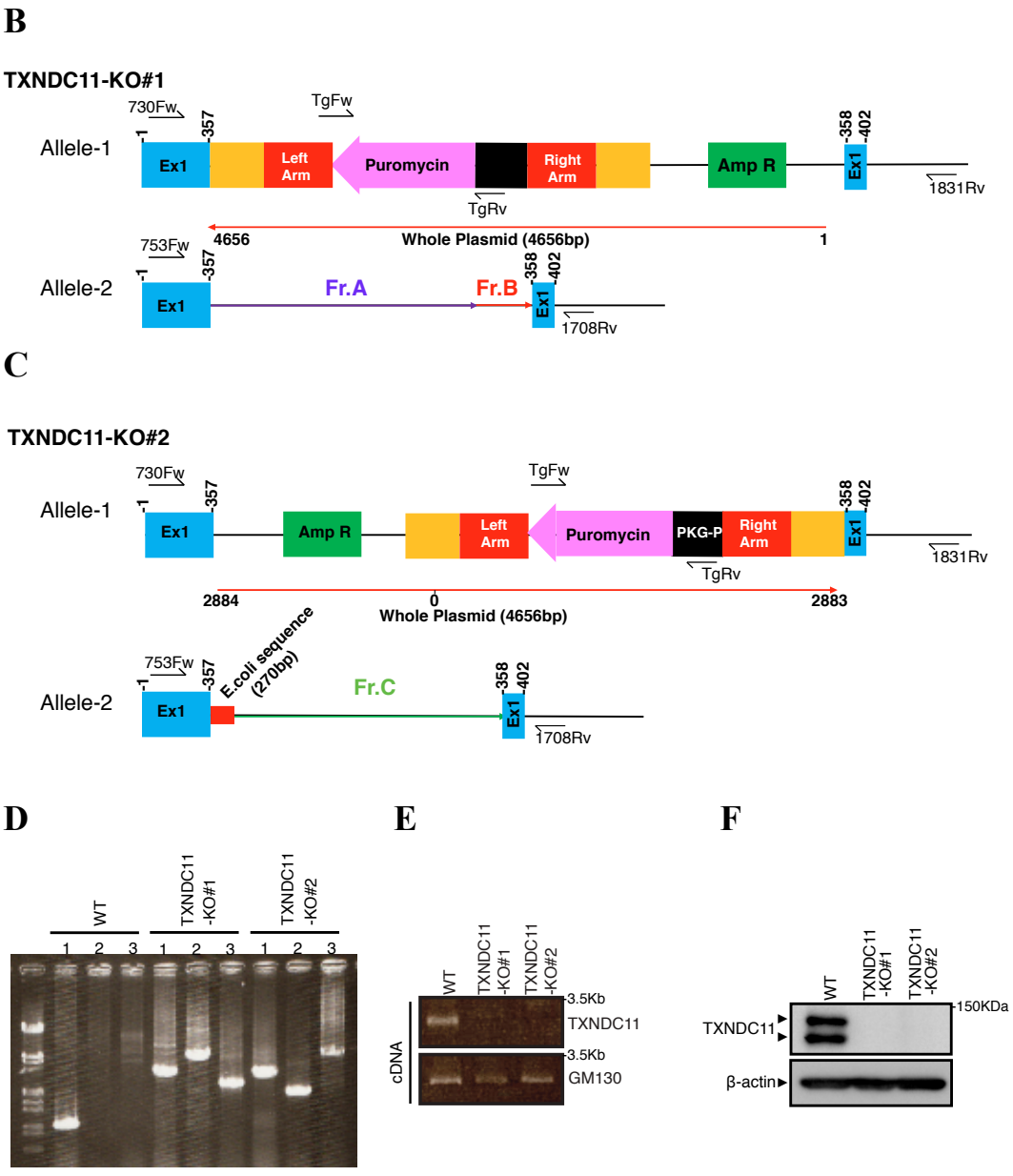

Figure 4 continued.

(B) Structures of the *TXNDC11* locus in TXNDC11-KO#1 cells are schematically shown. **(C)** Structures of the *TXNDC11* locus in TXNDC11-KO#2 cells are schematically shown. **(D)** Genomic PCR was carried out to confirm recombination. Primers for lanes 1, 2 and 3 are 753Fw and 1708Rv, TgFw and 1831Rv, and 730Fw and TgRv, respectively. **(E)** Total RNA was prepared from WT and two TXNDC11-KO cells, and subjected to RT-PCR to amplify cDNA corresponding to full length TXNDC11 and GM130. **(F)** Cell lysates were prepared from WT and two TXNDC11-KO cells, and analyzed by immunoblotting using anti-TXNDC11 and β-actin antibodies.

Evaluation of Cas9 activity remained in TXNDC11-KO cells.

To rule out the possibility of Cas9 activity remained in newly constructed TXNDC11-KO cells, I cloned the target region of *TXNDC11* gene into the pCAG-EGxxFP vector. In this vector, the enhanced green fluorescent protein (EGFP) gene is split into two inactive fragments containing overlapping homologies (Clavel et al.,1986). In cells, cleavage at the TXNDC11 target site by Cas9 initiates single strand annealing and generates an active EGFP gene. Co-transfection of the pCAG-EG-TXNDC11-FP and pX330A-TXNDC11-PITChx2 vectors lead to enhanced EGFP fluorescence (Fig. 5A, B and C). However, the sole transfection of pCAG-EG-TXNDC11-FP vector did not lead to EGFP fluorescence, indicating that there was no significant Cas9 activity remained in either of the TXNDC11-KO cells (Fig. 5A, B and C).

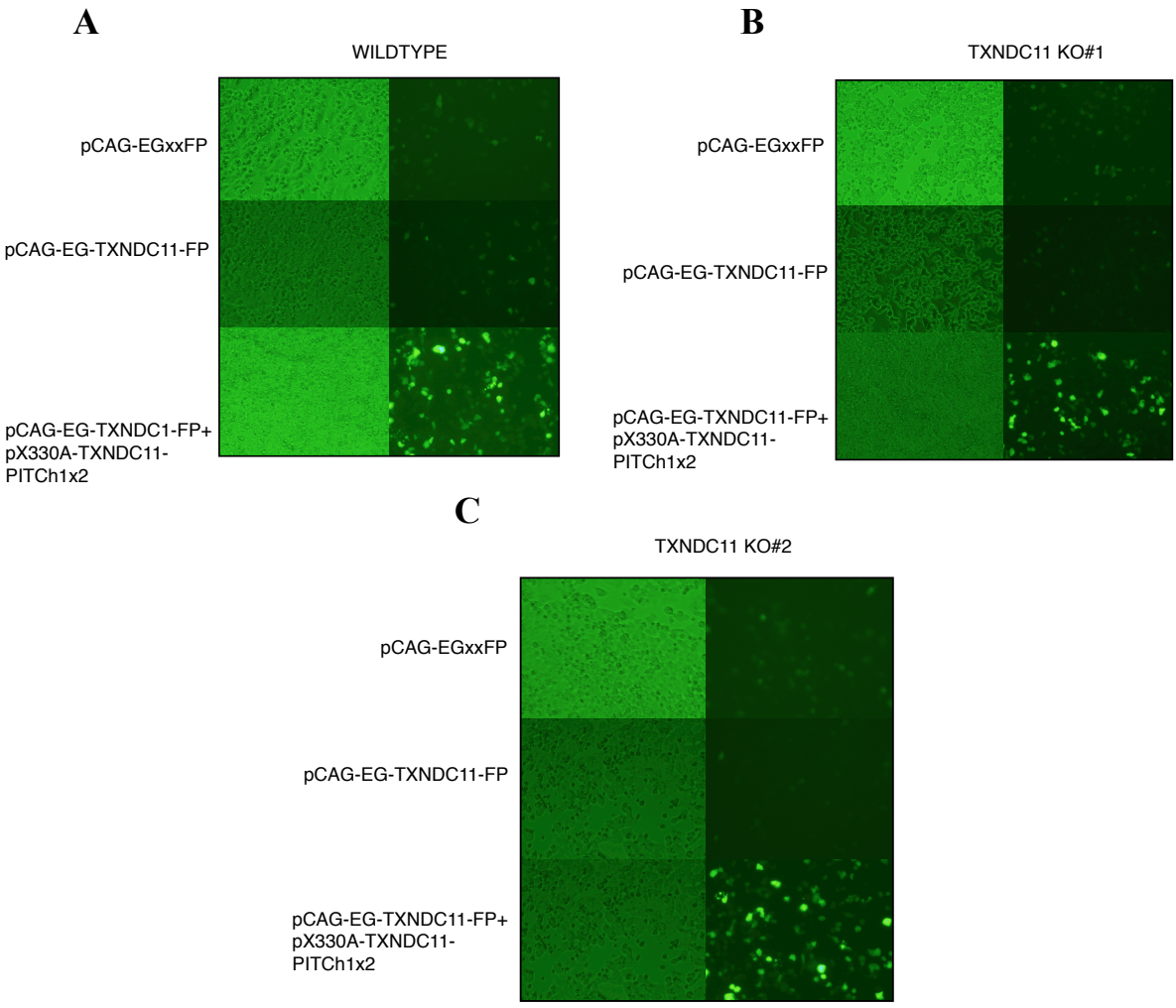

Figure 5: Evaluation of Cas9 activity remained in TXNDC11-KO cells.

(A), (B), (C). WT and two TXNDC11-KO cells were transfected with pCAG-EGxxFP pCAG-EG-TXNDC11-FP or both pCAG-EG-TXNDC11-FP and pX330A-TXNDC11-PITChx2 vectors, and observed for EGFP fluorescence using confocal microscopy after 48h.

TXNDC11-EDEM2 complex is essential for gpERAD

The immunoblotting clearly showed that higher molecular weight forms of EDEM2 completely disappeared in both TXNDC11-KO cells (Fig. 6A). Co-expression of Flag-tagged TXNDC11 and Myc-his-tagged EDEM2 lead to reappearance of the higher molecular weight bands which were specific to both anti-EDEM2 and anti-TXNDC11 antibodies (Fig. 6B). Both the TXNDC11-KO cells showed the defect in mannose trimming of mCD3-δ-ΔTM-HA (Fig. 6C). This defect was restored by the external co-expression of Flag-tagged TXNDC11 with mCD3-δ-ΔTM-HA (Fig. 6C). Moreover, similarly to EDEM2-KO cells, the degradation of mCD3-δ-ΔTM-HA was significantly delayed in TXNDC11-KO#1 and TXNDC11-KO#2 cells in contrast to WT cells (Fig. 6E). It was shown that the degradation of endogenous ATF6α, a type II transmembrane glycoprotein in the ER, was initiated by EDEM2-mediated mannose trimming (Ninagawa et al., 2014). The degradation of ATF6α was also delayed in both TXNDC11-KO cells as compared to WT cells (Fig. 6D). N-glycan profiling showed that M9 oligosaccharide was markedly accumulated in TXNDC11-KO cells, comparably to that in EDEM2-KO cells (Fig. 6F and G). Thus, these results collectively indicate that the EDEM2-TXNDC11 complex is involved in first mannose trimming, and is vital for gpERAD initiation.

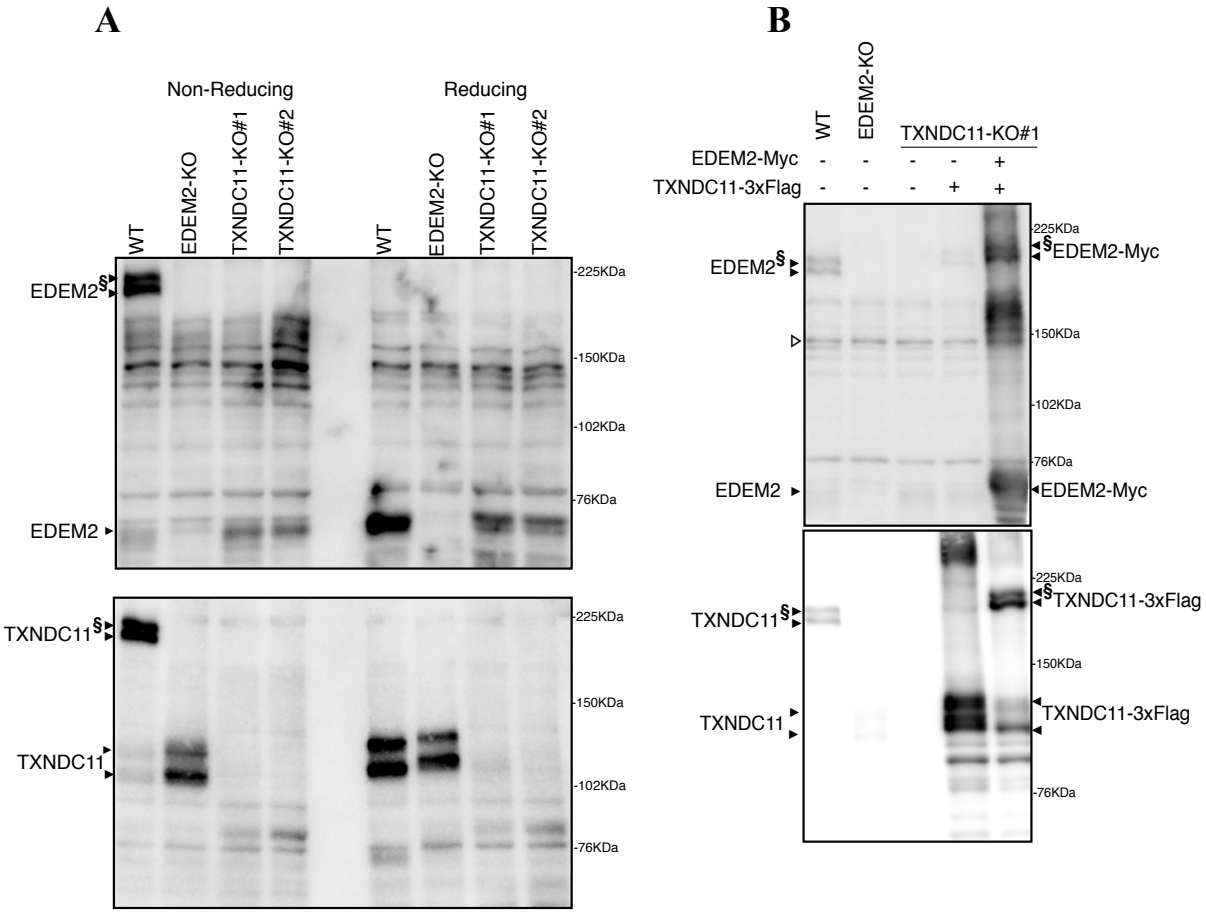

Figure 6: TXNDC11-EDEM2 complex is essential for gpERAD

(A) Cell lysates were prepared from WT, EDEM2-KO, and two TXNDC11-KO cells, subjected to SDS-PAGE under reducing and non-reducing conditions, and analyzed by immunoblotting using anti-EDEM2 and anti-TXNDC11 antibodies. **(B)** Cell lysates were prepared from WT, EDEM2-KO, and TXNDC11-KO#1 cells expressing 3x Flag-tagged TXNDC11 or both 3xFlag-tagged TXNDC11 and Myc-tagged EDEM2 by transfection, subjected to SDS-PAGE under non-reducing conditions, and analyzed by immunoblotting using anti-EDEM2 and anti-TXNDC11 antibodies.

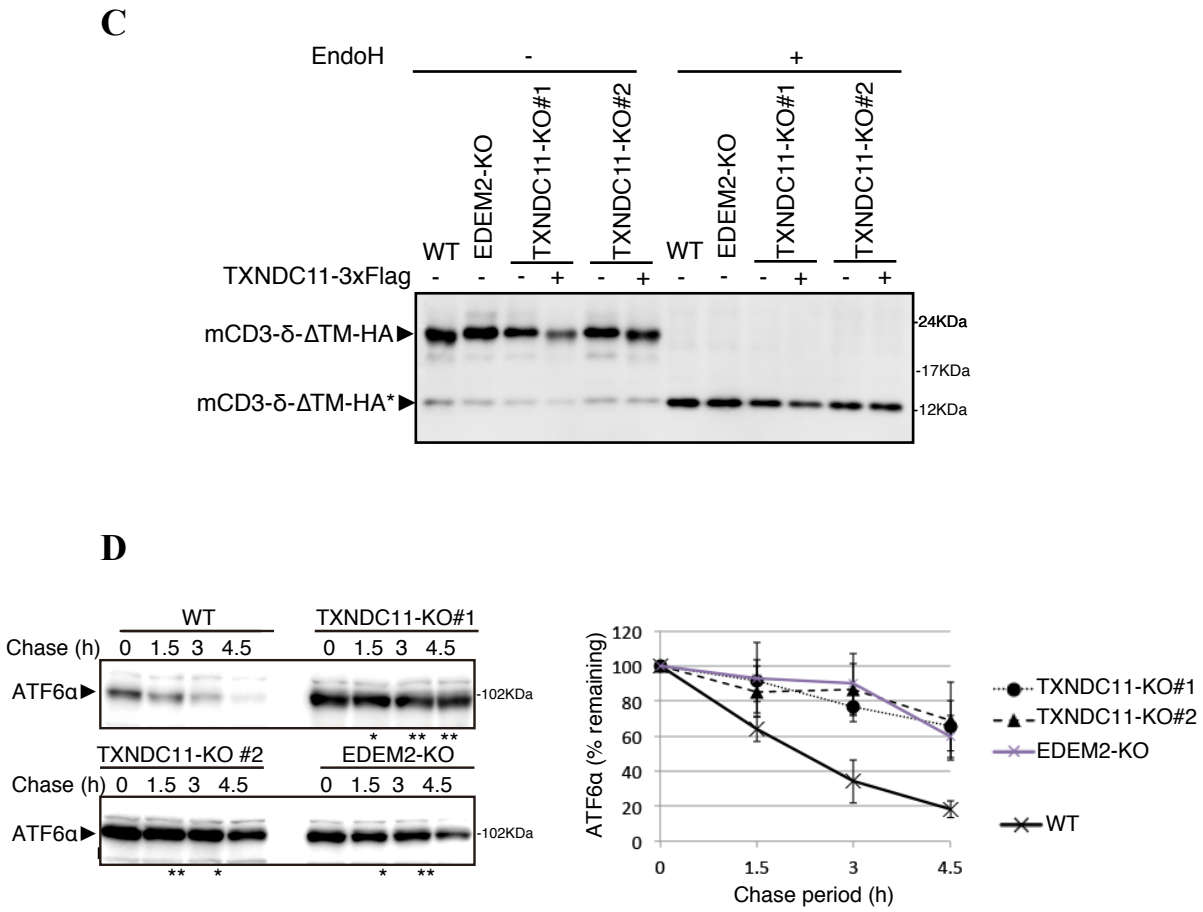

Figure 6 continued.

(C) WT and EDEM2-KO cells were transfected with the plasmid to express mCD3-δ-ΔTM-HA. Two TXNDC11-KO cells were also transfected with the plasmid to express mCD3-δ-ΔTM-HA together with (+) or without (-) the plasmid to express 3xFlag-tagged TXNDC11(WT). Cell lysates were then prepared, treated with (+) or without (-) EndoH, and analyzed by immunoblotting using anti-HA antibody. **(D)** Cycloheximide chase was conducted to determine the degradation rate of endogenous ATF6α in WT, EDEM2-KO and two TXNDC11-KO cells, and cell lysates were analyzed by immunoblotting using anti-ATF6α antibody (n=3). Quantified data are shown on the right.

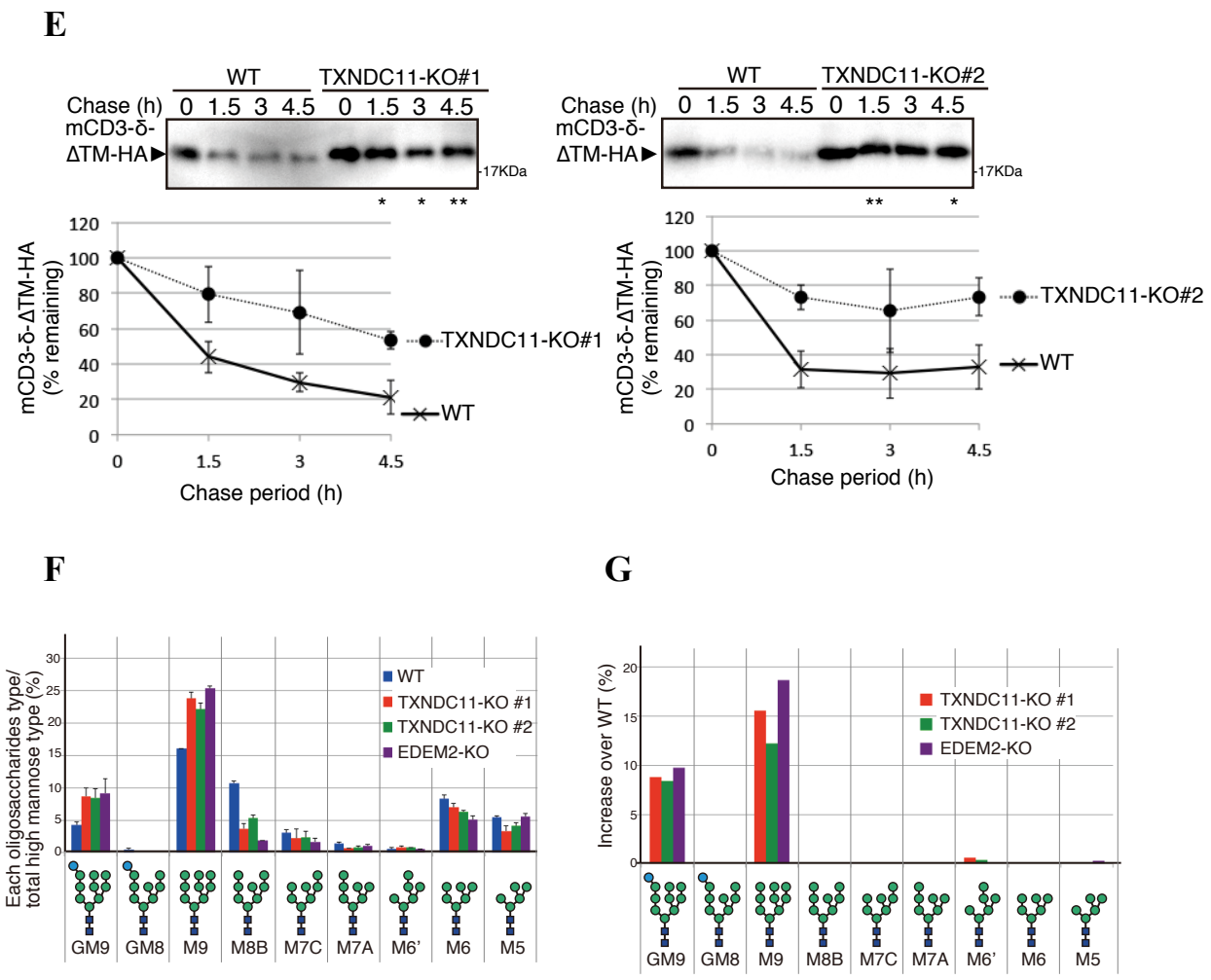

Figure 6 continued.

(E) Cycloheximide chase was conducted to determine the degradation rate of mCD3-δ-ΔTM-HA in transfected WT and two TXNDC11-KO cells, and cell lysates were analyzed by immunoblotting using anti-HA antibody (n=3). Quantified data are shown below. **(F)** Isomer composition of N-glycans prepared from total cellular glycoproteins of WT, TXNDC11-KO#1, TXNDC11-KO#2 and EDEM2-KO cells is shown. **(G)** Oligosaccharides obtained in (A) whose contents in TXNDC11-KO#1, TXNDC11-KO#2 and EDEM2-KO cells exceeded those in WT cells are displayed with the increase over WT (%).

TXNDC11 uses alternative translation to produce its membrane and soluble versions.

TXNDC11, a type II transmembrane protein, has a single transmembrane domain (TMD) at the N- terminus followed by five thioredoxin (Trx)-like domains and a coiled coil domain. It also has ten predicted N-glycosylation sites (Fig. 7A).

Immunoblotting showed that TXNDC11 is always detected as a doublet band in SDS-PAGE and both bands are N-glycosylated (Fig. 7B). We noticed that the TXNDC11 bands migrated more slowly in EDEM2-KO cells than in WT and that this difference disappeared after treatment with EndoH (Fig. 7B). The protein sequence of TXNDC11 showed two methionine residues (M1 and M58) at the N-terminus just before the TMD (Fig. 7A). As the DNA sequence around both M1 (catGtaATGt) and M58 (ttcctcATGG) resembles the Kozak consensus sequence for translational initiation (gccRccATGG), I sought the possibility that translation started at two methionine residues. To pursue this possibility, I mutated M1 and M58 to alanine and transfected the mutated plasmid into TXNDC11-KO cells separately. The band pattern in the immunoblot clearly showed that the M1A mutant had only one, which is longer version, and that M58A also had only a single band with shorter version (Fig. 7C). Both forms can stimulates the EDEM2 mannosidase activity, as mCD3-δ-ΔTM-HA migrated faster in TXNDC11-KO cells expressing M1A and M58A with mCD3-δ-ΔTM-HA, similarly to the case of WT TXNDC11 (Fig. 7D).

I have performed freeze and thaw experiment followed by centrifugal fractionation to separate the membrane and soluble portions of whole lysates. The results clearly showed that the M58A mutant is a membrane version of TXNDC11, similarly to calnexin, and that the M1A mutant is the soluble protein (Fig. 7E). Thus, membrane and soluble versions of TXNDC11 are produced by alternative translation initiation. This suggests that TMD acts as a relatively weak signal peptide for M1A. SignalP-5.0 (http://www.cbs.dtu.dk/services/SignalP/) predicted that the probability for functionality of the TMD as a signal peptide is between 0.6 and 0.7 and that the probability for its cleavage at the C-terminus of A87 is approximately 0.5 (Fig. 7F). I therefore constructed the ΔSP (lacking amino acids from A59 to A87; see Fig. 7A) and A87F (having the probability for functionality of the TMD as a signal peptide and the probability for its cleavage of less than 0.4 and approximately 0.1, respectively; Fig. 7F) mutants in the M1A mutant and introduced them into TXNDC11-KO cells separately. M1A-ΔSP was synthesized as an unglycosylated cytosolic protein, as expected (Fig. 7G). M1A-A87F moved slightly slower than M1A before and after EndoH treatment during reducing SDS-PAGE (Fig. 7G) and M1A-A87F was mostly a calnexin-like membrane protein (Fig. 7H). I

concluded that M1A becomes a soluble protein if it is cleaved by signal peptidase and that M1A uncleaved by chance remains as a M58A-like membrane protein.

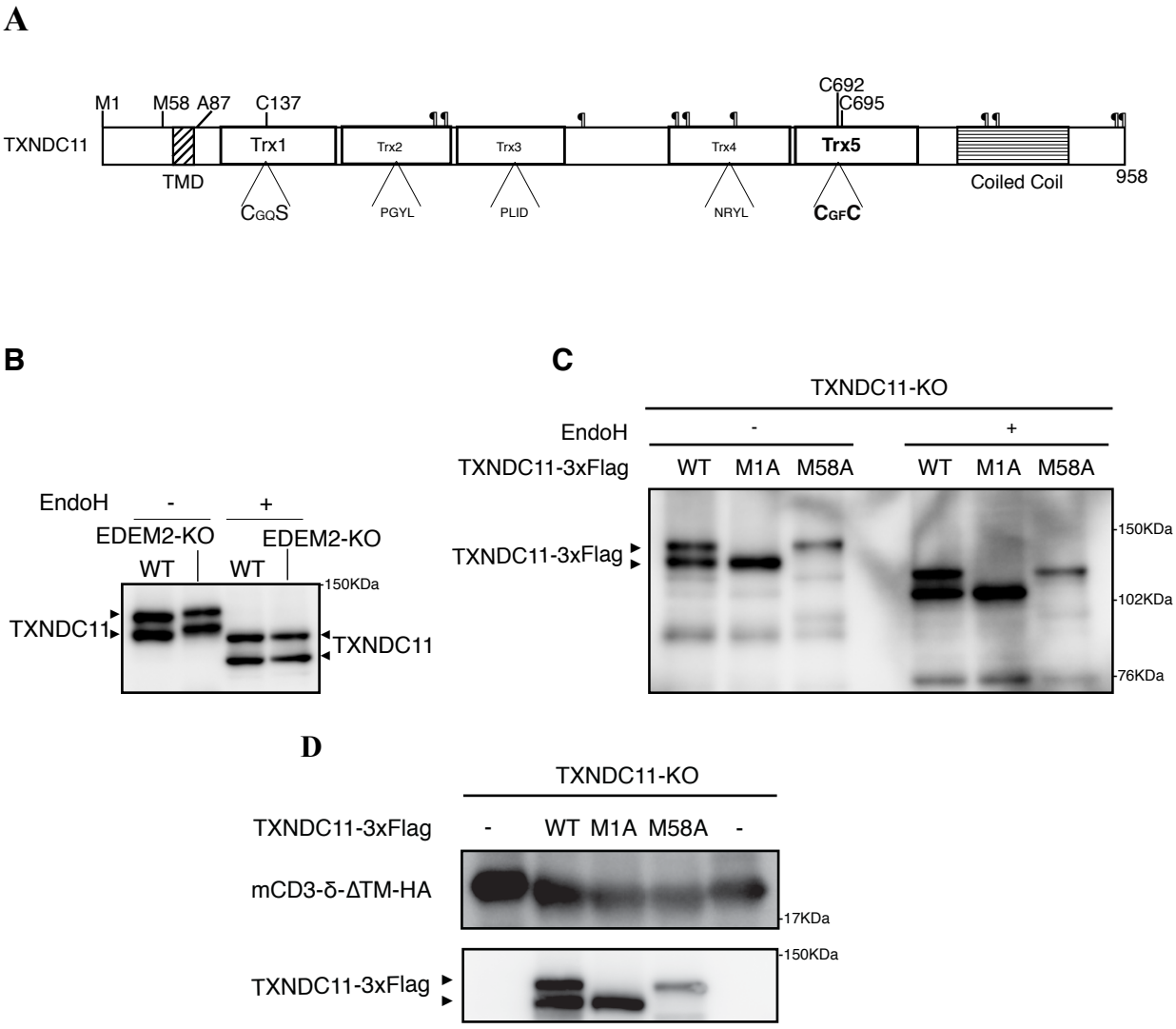

Figure 7: TXNDC11 uses alternative translation to produce its membrane and soluble versions.

(A) Structure of human TXNDC11 containing the TMD, five Trx domains, and coiled coil domain is schematically shown. ¶ denotes potential N-glycosylation sites. The positions of the two initiation methionines are also shown. **(B)** Cell lysates prepared from WT and EDEM2-KO cells, treated with (+) or without (-) EndoH, and analyzed by immunoblotting using anti-TXNDC11 antibody. **(C)** Cell lysates were prepared from TXNDC11-KO cells expressing WT, M1A or M58A mutant of 3x Flag-tagged TXNDC11 by transfection, treated with (+) or without (-) EndoH, and analyzed by immunoblotting using anti-Flag antibody. **(D)** Cell lysates were prepared from TXNDC11-KO cells expressing mCD3-δ-ΔTM-HA together with the WT, M1A, or M58A mutant of 3x Flag-tagged TXNDC11 by transfection, and analyzed by immunoblotting using anti-TXNDC11 and anti-HA antibodies.

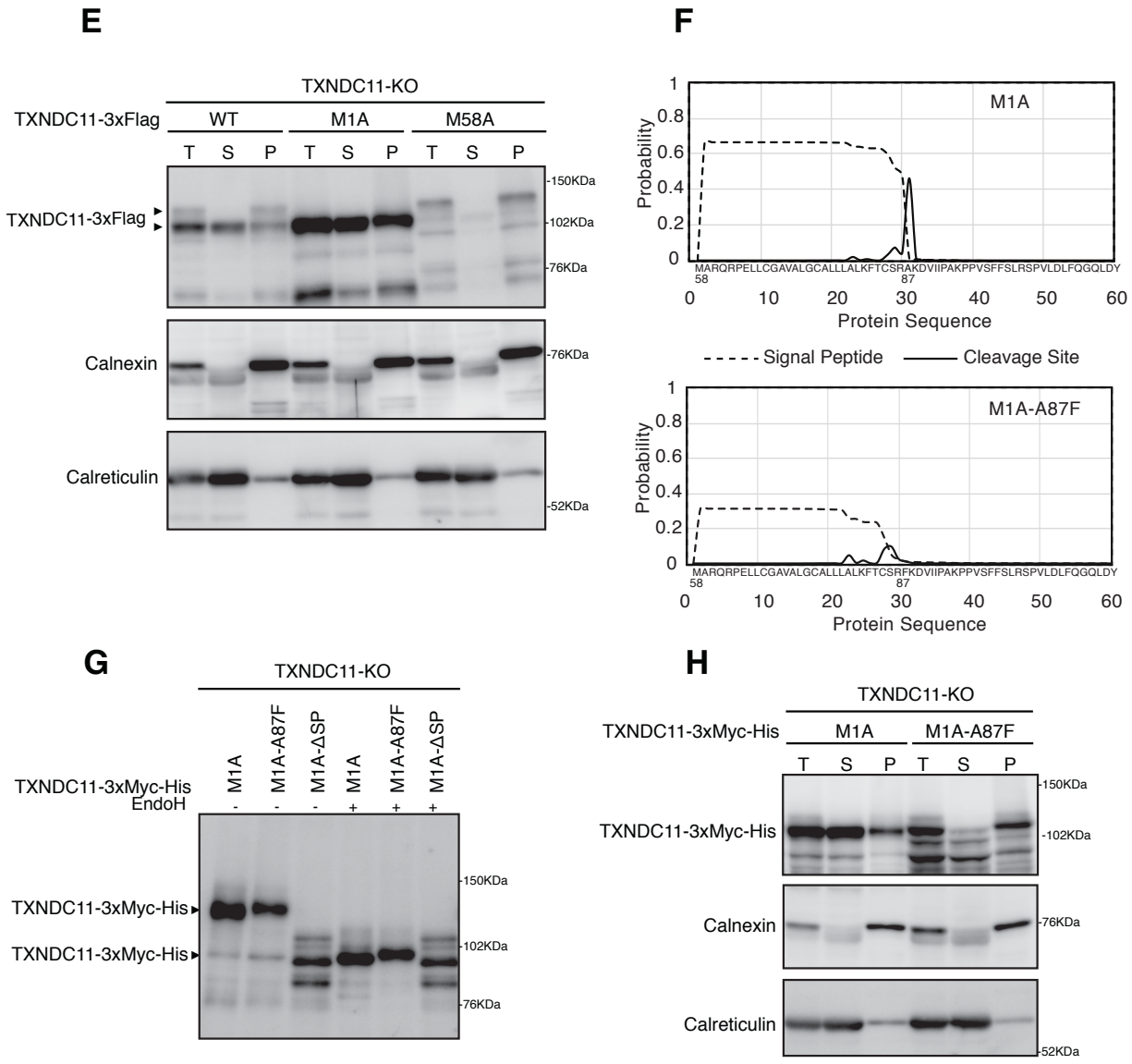

Figure 7 continued.

(E) Cell lysates were prepared from WT and TXNDC11-KO cells expressing the M1A or M58A mutant of 3x Flag-tagged TXNDC11 by transfection, and subjected to repeated freezing and thawing. An aliquot of total membrane fraction (T) and resulting supernatant (S) and precipitate (P) were analyzed by immunoblotting using anti-TXNDC11, anti-calnexin and anti-calreticulin antibodies. **(F)** SignalP-5.0-mediated prediction of the probability for functionality of the TMD as a signal peptide (broken line) and the probability for its cleavage by signal peptidase (solid line) of M1A (upper) and M1A-A87F (lower). **(G)** Cell lysates were prepared from TXNDC11-KO cells expressing M1A, M1A-A87F, or M1A-ΔSP mutant of 3x Myc-His-tagged TXNDC11 by transfection, treated with (+) or without (-) EndoH, and analyzed by immunoblotting using anti-TXNDC11 antibody. **(H)** TXNDC11-KO cells expressing M1A or M1A-A87F mutant of 3x Myc-His-tagged TXNDC11 by transfection were analyzed as in (C).

Requirement of cysteine residues of TXNDC11 for EDEM2 mannosidase activity

A previous report suggested the possibility of reductase activity of TXNDC11, in which C692 and C695 present in the CxxC motif of the active thioredoxin 5 domain were important for its function (Timms et al., 2016). I decided to explore in more detail the importance of cysteines in TXNDC11 for its function in regard to EDEM2 mannosidase activity.

TXNDC11 contains 24 cysteine residues (Fig. 8A). To identify the important cysteines involved in TXNDC11 function, I mutated each cysteine residue to serine, co-expressed with mCD3-δ-ΔTM-HA, and checked the migration pattern of mCD3-δ-ΔTM-HA. The results showed that there were five important cysteines (highlighted in red color), C165, C172, C380, C574 and C692, and that their mutation to serine lead to slower migration of mCD3-δ-ΔTM-HA, indicating that these cysteines are essential for TXNDC11 function in terms of EDEM2 activity (Fig. 8B). Interestingly, the cysteine present in the CxxS motif (C137) and one of the two cysteines in the canonical CxxC motif (C695) did not seem to be important, as their mutation to serine did not change the migration of mCD3-δ-ΔTM-HA (Fig. 8B).

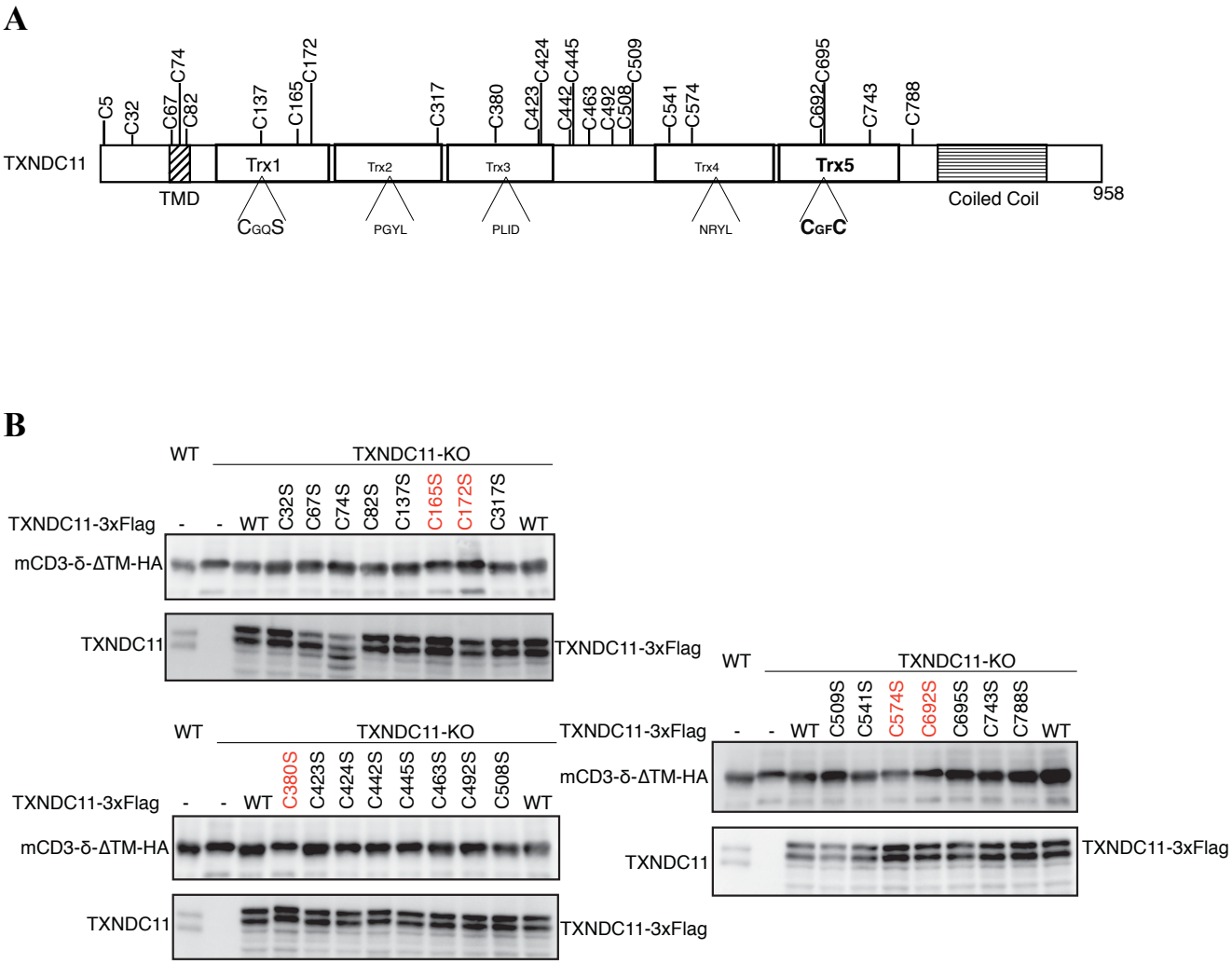

Figure 8: Requirement of cysteine residues of TXNDC11 for the EDEM2 mannosidase activity.

(A) Structure of human TXNDC11 is schematically shown with cysteine residues (C) highlighted together with their positions. **(B)** Cell lysates were prepared from WT and TXNDC11-KO cells expressing WT or each cysteine mutant of 3x-Flag-tagged TXNDC11 together with mCD3-δ-ΔTM-HA by transfection, and analyzed by immunoblotting using anti-HA and anti-TXNDC11 antibodies.

TXNDC11 stably interacts with EDEM2 via C692 residue present in the canonical Trx5 domain.

To identify which cysteine of TXNDC11 is important for inter-disulfide bond formation with C558 of EDEM2, I co-transfected each cysteine mutant with Myc-his tagged EDEM2 in TXNDC11-KO cells. Non-reducing SDS-PAGE followed by immunoblotting analysis showed that disulfide-mediated higher molecular weight complex formation was disrupted in cells expressing the Flag-tagged C692S of TXNDC11 with Myc-his-tagged EDEM2 (Fig. 9A, third panel). This result was further confirmed by immunoprecipitation in cells expressing WT or one of the three cysteine mutants present in the Trx1 and Trx5 domains of TXNDC11 (Fig. 9B). Consistent with the defect in complex formation, the C692S mutant expressed in TXNDC11-KO cells did not restore in vivo EDEM2 mannosidase activity (Fig.9C) as well as gpERAD of mCD3-δ-ΔTM-HA, in contrast to WT or C137S, C695S version of TXNDC11 (Fig. 9D).

A

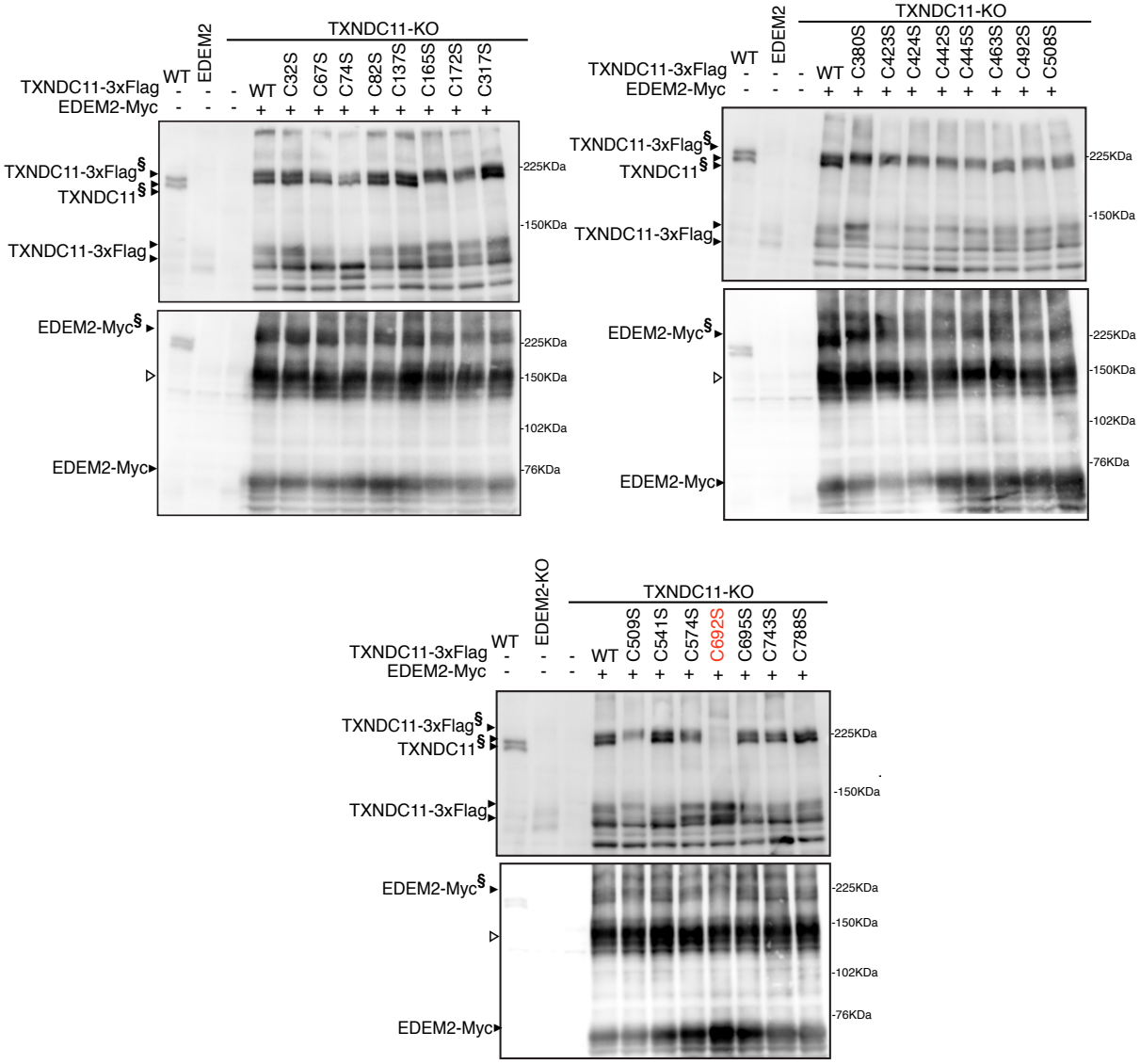

Figure 9: TXNDC11 stably interacts with EDEM2 via the C692 residue present in the canonical Trx5 domain.

(A) Cell lysates were prepared from WT, EDEM2-KO, and TXNDC11-KO cells expressing WT or one of various cysteine mutants of 3x Flag-tagged TXNDC11 together with Myc-tagged EDEM2 by transfection, subjected to SDS-PAGE under non-reducing conditions, and analyzed by immunoblotting using anti-TXNDC11 and anti-EDEM2 antibodies.

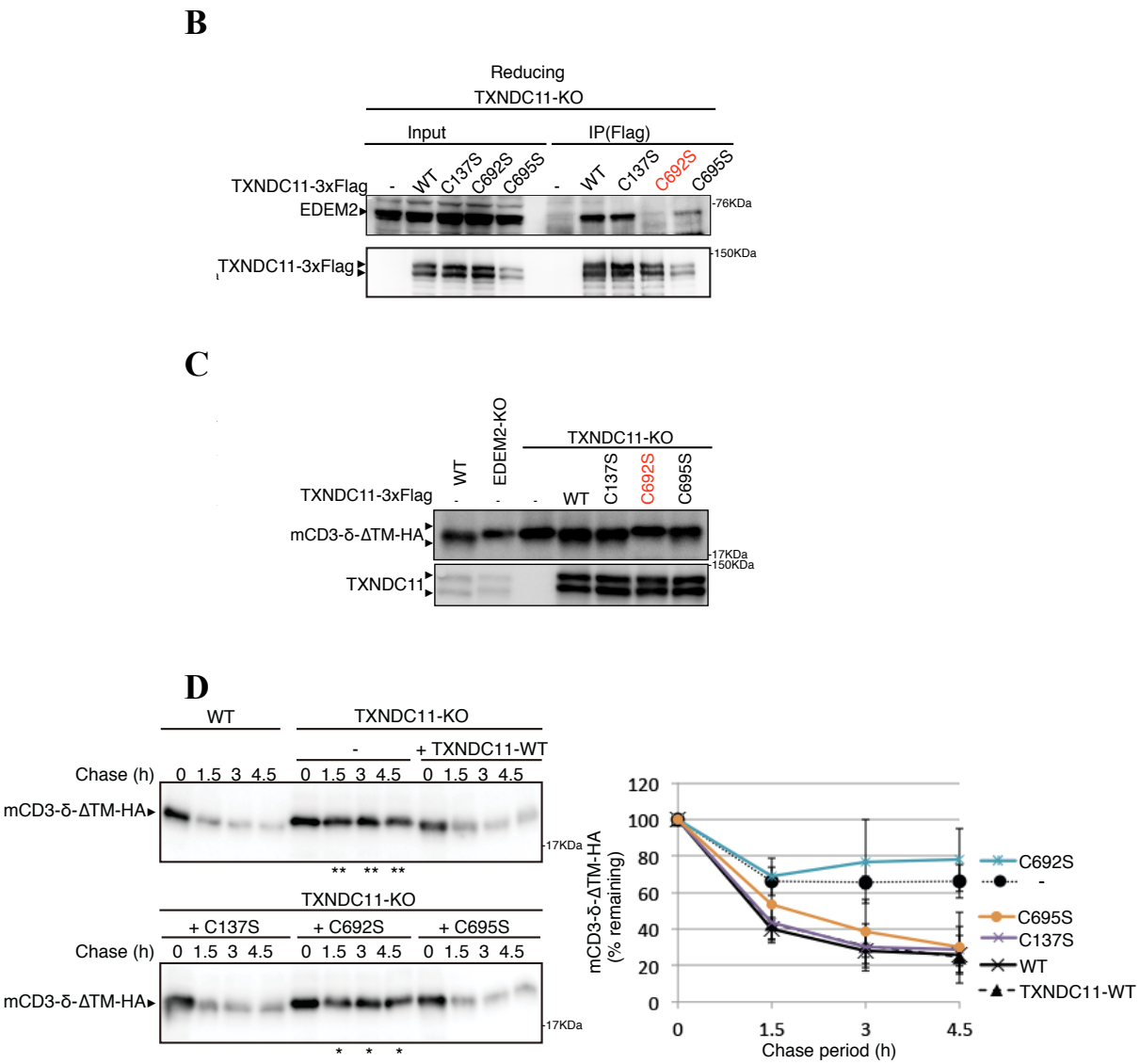

Figure 9 continued.

(B) Cell lysates were prepared from TXNDC11-KO cells expressing WT or one of the three cysteine mutants of 3x Flag-tagged TXNDC11 and subjected to immunoprecipitation using anti-Flag antibody. Aliquots of cell lysates (Input) and the immunoprecipitates {IP(Flag)} were subjected to SDS-PAGE under reducing conditions and analyzed by immunoblotting using anti-EDEM2 and anti-TXNDC11 antibodies. **(C)** Cell lysates were prepared from WT, EDEM2-KO, and TXNDC11-KO cells expressing WT or one of the three cysteine mutants of 3x Flag-tagged TXNDC11 together with mCD3-δ-ΔTM-HA by transfection and analyzed by immunoblotting using anti-HA and anti-TXNDC11 antibodies. **(D)** Cycloheximide chase was conducted to determine the degradation rate of mCD3-δ-ΔTM-HA in WT and TXNDC11-KO cells expressing WT or one of the three cysteine mutants of 3x Flag-tagged TXNDC11 by transfection, and cell lysates were analyzed by immunoblotting using anti-HA antibody (n=3). Quantified data are shown on the right.

EDEM2 exists in different conformation in the absence of stable binding with TXNDC11

It is important to know how TXNDC11 helps maintaining the mannosidase activity of EDEM2. Immunoblotting analysis showed there was a lower amount of EDEM2 monomer in TXNDC11-KO cells (Fig. 6A, reducing). However, in quantitative RT-PCR, the level of *EDEM2* mRNA was not affected by the TXNDC11 knock out (Fig. 10A). The similar level of spliced *XBP1* mRNA in WT and TXNDC11-KO cells indicated that there was no ER stress induction in the absence of TXNDC11 (Fig. 10A). The cycloheximide chase experiment suggested that in contrast to WT cells, the endogenous EDEM2 degradation was enhanced in TXNDC11-KO cells (Fig. 10B). Importantly, the higher molecular weight forms of EDEM2 present in the WT cells were more resistant to trypsin digestion than the EDEM2 monomer present in TXNDC11-KO cells (Fig. 10C). This suggests that EDEM2 attains a different conformation with and without TXNDC11.

A

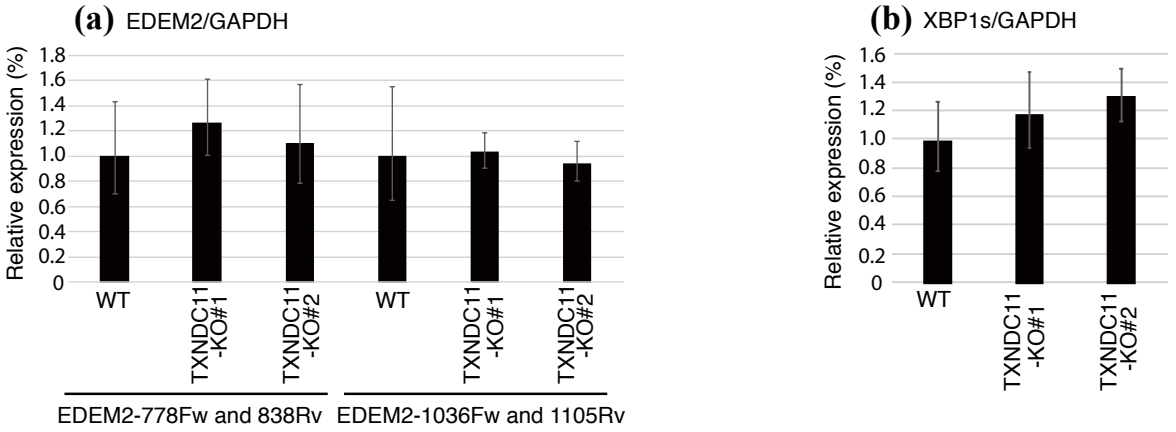

B

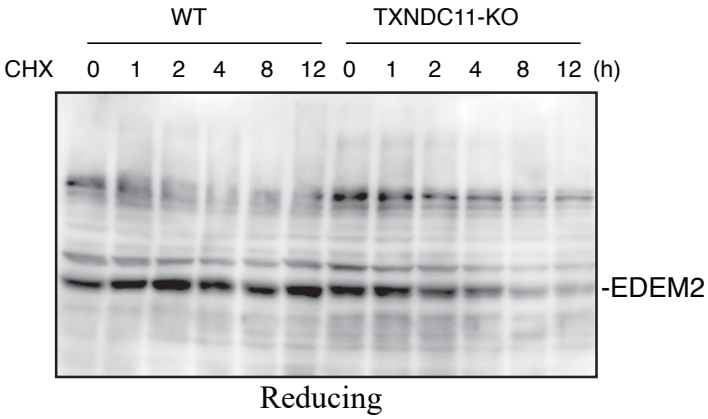

Figure 10: EDEM2 exists in a different conformation in the absence of stable binding with TXNDC11

(A) Quantitative RT-PCR was conducted to determine the levels of endogenous *EDEM2* mRNA **(a)** using the two primer sets indicated as well as spliced *XBP1* mRNA **(b)** relative to the level of *GAPDH* mRNA in WT and two TXNDC11-KO cells (n=3). **(B)** Cycloheximide chase was conducted to determine the degradation rate of EDEM2 in WT and TXNDC11-KO cells. The cell lysates were prepared and analyzed by immunoblotting using anti-EDEM2 antibody.

C

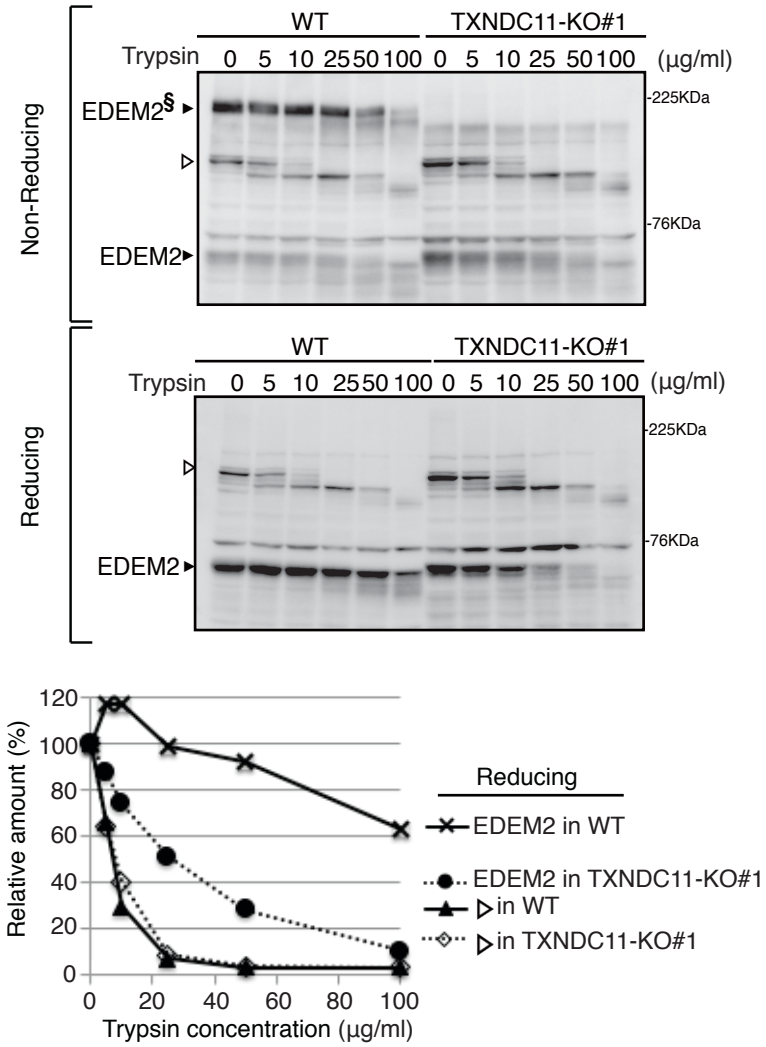

Figure 10 continued.

(C) Cell lysates were prepared from WT and TXNDC11-KO#1 cells, treated with the indicated amount of trypsin at 4°C for 15 min, subjected to SDS-PAGE under reducing and non-reducing conditions, and analyzed by immunoblotting using anti-EDEM2 antibody. The band with the open triangle denotes a non-specific protein which serves as a control for trypsin digestion. Quantified data are shown at the bottom.

Evaluation of disulfide formation of EDEM2 in WT and TXNDC11-KO cells

Previous study suggested that the redox activity of TXNDC11 is important for ERAD function (Timms et al., 2016). As TXNDC11 forms a stable complex with EDEM2, I decided to check the effect of TXNDC11 on EDEM2 oxidative state, especially the bond between C65 and C408 in the MHD. I treated the lysates from WT, TXNDC11-KO and EDEM2-KO cells with NEM to modify free cysteines, followed by DTT incubation to reduce the disulfide-bonded cysteines, and then incubation with DNA-maleimide. The immunoblotting after maleimide modification showed five EDEM2-specific bands with different molecular weights indicating that the chemical modification was not uniform (Fig. 11A). However, the topmost EDEM2 specific band in WT - in contrast to TXNDC11-KO cells - suggested the possible C558 maleimide modification (Fig. 11 A). Nevertheless, there was no difference in band pattern other than C558 maleimide modification, suggesting that TXNDC11 does not affect the oxidation state of EDEM2.

To evaluate the C65-C408 disulfide bond formation, I wanted to perform mass spectrometric analysis by focusing on peptides containing C65 and C408. To this end, I co-expressed Flag-tagged TXNDC11(M1A) with WT or the C558A mutant of tandem affinity purification (TAP)-tagged EDEM2 in EDEM2-KO cells. I also expressed TAP-EDEM2 WT in TXNDC11-KO cells. The purification methods were described later. To prepare the samples for mass spectrometric analysis, I performed negative staining under non-reducing conditions, followed by gel cutting of specific bands corresponding to EDEM2 monomer and EDEM2-TXNDC11 complex (Fig.11 B). To generate peptide fragments, trypsin-mediated digestion in gel was performed, and the reaction products were then treated with endoproteinase Asp-N. The final peptide fragments were subjected for further analysis. The results showed that the majority of EDEM2- and TXNDC11-specific peptides were in the 6^{th} portion of the gel (Fig. 11C). Although there were many peptides which contained C65 and C408, no peptide was detected in which C65 and C408 were disulfide bonded (Fig. 11 D and E).

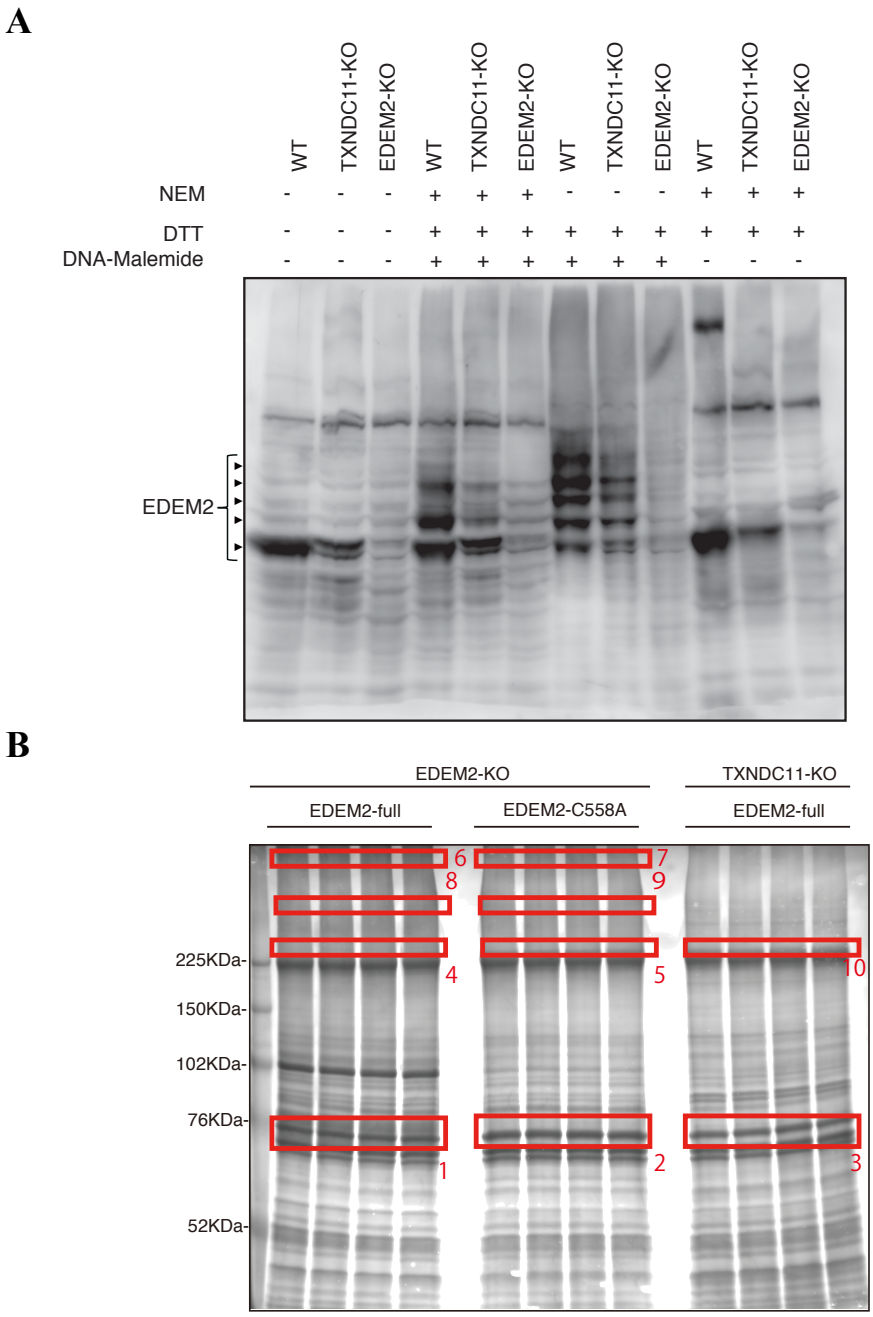

Figure 11: Evaluation of disulfide formation of EDEM2 in WT and TXNDC11-KO cells

(A) Cell lysates from WT, EDEM2-KO and TXNDC11-KO cells were precipitated with TCA and solubilized by sonication. The samples were incubated with (+) or without (-) NEM for 30 min at 37ºC and then treated with (+) or without (-) DTT. The DTT were removed by TCA precipitation and the pellet was solubilized by sonication. Aliquots of final samples were treated with (+) or without (-) DNA-Maleimide for 30 min at 37ºC and subjected to SDS-PAGE. The DNA tag was removed by incubating the gel under UV for 15 min followed by immunoblotting using anti-EDEM2 antibody. **(B)** EDEM2-KO and TXNDC11-KO cells were transfected with the indicated plasmids and subjected to purification by the TAP system as described later (Fig. 12A). Samples eluted from the beads by digestion with TEV protease were subjected to non-reducing SDS-PAGE and negative-staining. The highlighted portions of the gel were dissected and used for mass-spectrometry analysis.

C

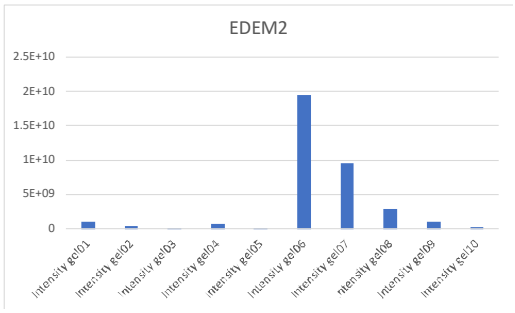

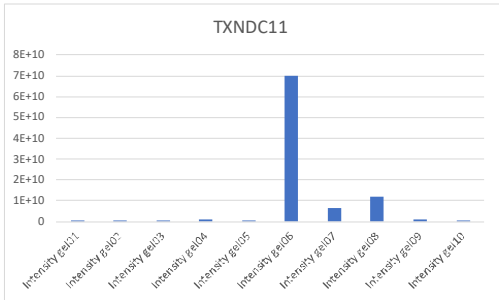

D

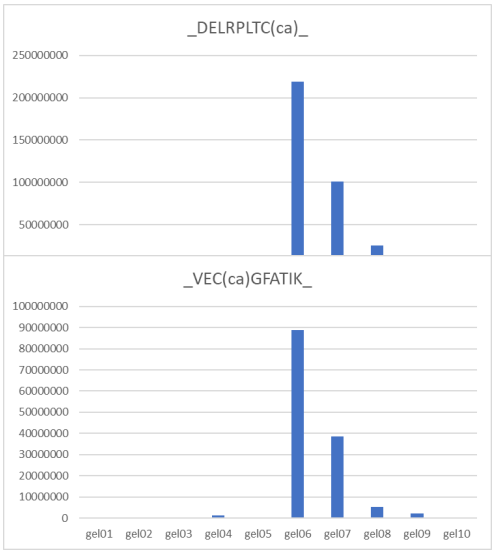

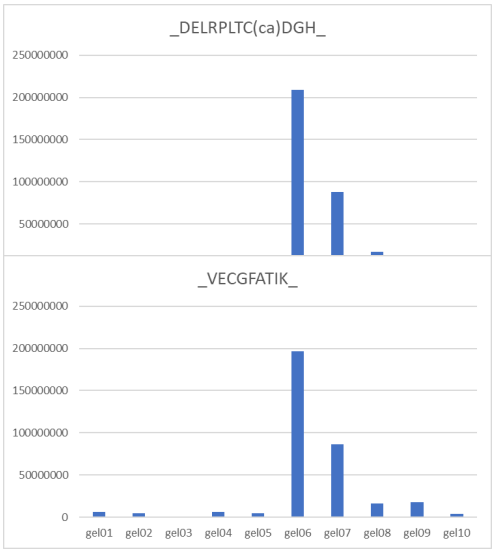

E

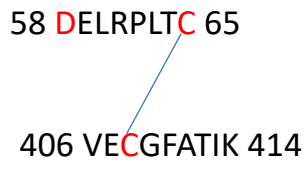

DELRPLTC	945.46
VECGFATIK	966.48
sum	1911.94
+2	956.97
+3	638.3133
+4	478.985

DELRPLTCDGH	1254.57
VECGFATIK	966.48
	2221.05
+2	1111.525
+3	741.35
+4	556.2625

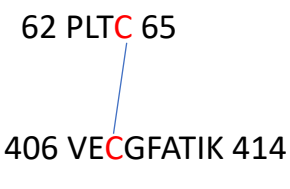

PLTC	432.2
VECGFATIK	966.48
	1398.68
2	700.34
3	467.2267
4	350.67

Figure 11 continued.

(C) Quantification of EDEM2- and TXNDC11-specific peptides detected by mass spectrometry. **(D)** Quantification of C65-and C408-specific peptides of EDEM2 detected by mass spectrometry. **(E)** Representation of predicted possible peptide containing C65 and C408 linkage theoretically, which was not detected in the peptide analysis. Ca denotes cysteine carbamidomethyl by IAA.

Purification of EDEM2-TXNDC11 complex

To determine in vitro mannosidase activity of EDEM2-TXNDC11 complex, it is important to obtain a sufficiently purified complex. I co-expressed Flag-tagged TXNDC11(M1A) with WT or C558A mutant of TAP-tagged EDEM2 in EDEM2-KO cells. TAP-tag contains 2x immunoglobulin binding site of protein A, 2xTEV protease recognition site and 6xMyc. At 48 h after transfection, TAP-EDEM2 was collected from cell lysates by adding IgG sepharose beads, followed by elution of TAP-free 6xMyc-EDEM2 by digestion with TEV protease (Fig. 12A). I confirmed the purity using silver staining after reducing SDS-PAGE (Fig. 12B). The presence of TXNDC11 and EDEM2 was confirmed by immunoblotting with anti-EDEM2 and anti-TXNDC11 antibodies (Fig. 12C). TXNDC11(M1A)-3xFlag was purified with WT but not with C558A EDEM2 (Fig. 12B). Because a marginal amount of TXNDC11(M1A)-3xFlag was detected in the eluate of C558A EDEM2 (Fig. 12C), TXNDC11 might physically associate with EDEM2 even in the absence of disulfide bonding, albeit only slightly.

A

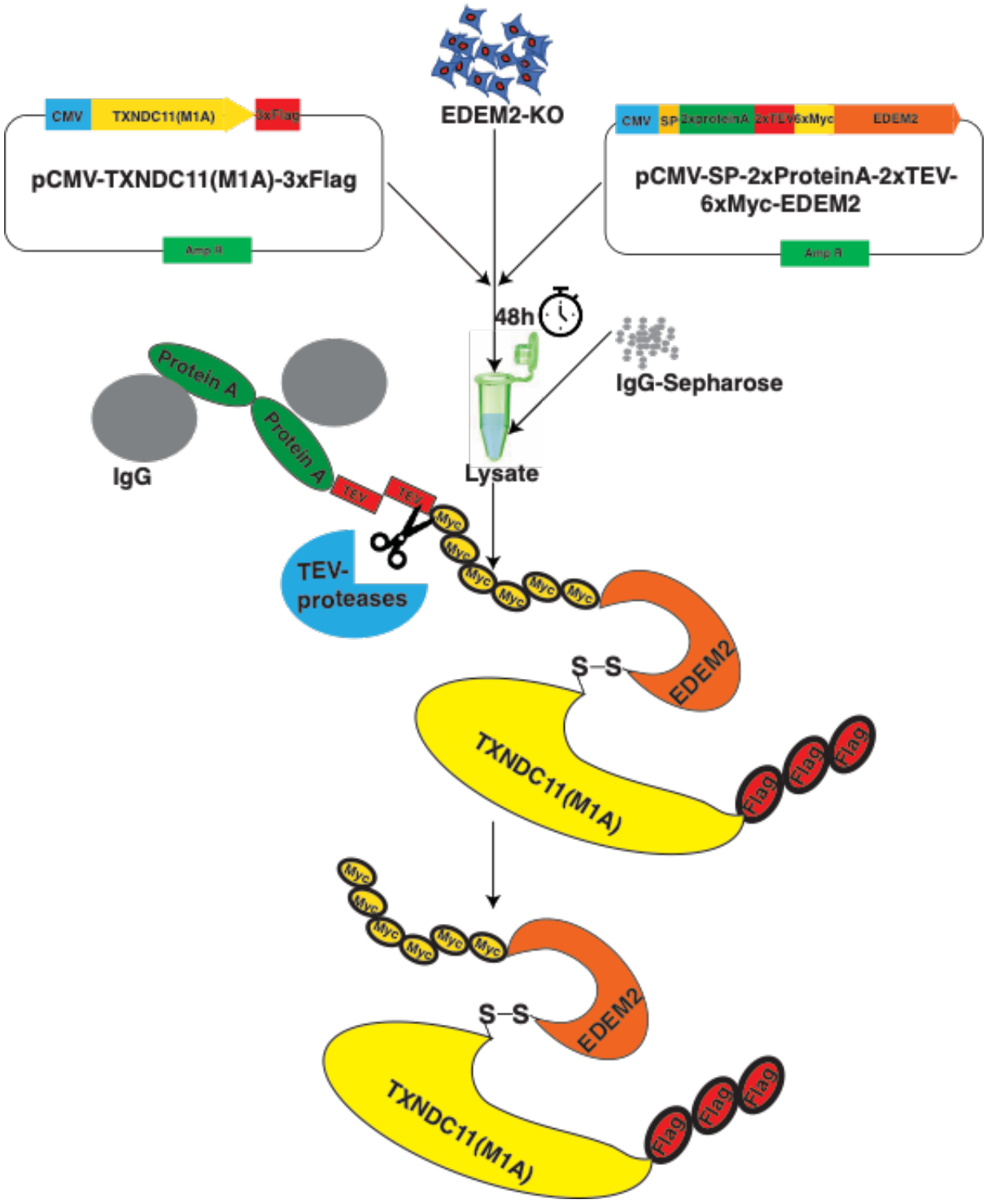

Figure 12: Purification of EDEM2-TXNDC11 complex

(A) Schematic representation of purification strategy of EDEM2-TXNDC11 complex.

B

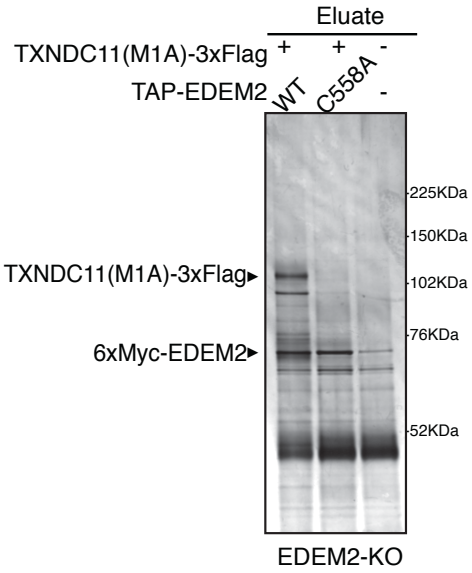

C

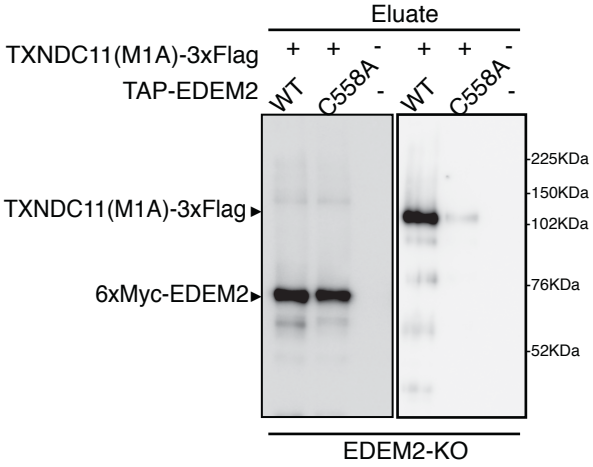

Figure 12 Continued.

(B) EDEM2-KO cells were untransfected (-) or transfected (+) with the indicated plasmids and subjected to purification using IgG Sepharose beads. Samples eluted from the beads by digestion with TEV protease were subjected to reducing SDS-PAGE and silver-staining. **(C)** The amounts of 6xMyc-EDEM2 and TXNDC11(M1A)-3xFlag in samples for in vitro assay were checked by immunoblotting using anti-EDEM2 and anti-TXNDC11 antibodies.

In vitro mannosidase activity of EDEM2-TXNDC11 complex

Equal amounts of purified EDEM2-TXNDC11(M1A) complex and EDEM2-C558A were incubated with pyridylaminated M9 (PA-M9) for various times. The results clearly showed that EDEM2-TXNDC11 complex extensively removed the mannose from PA-M9 and converted it to PA-M8 (Fig.13A). In contrast, EDEM2-C558A only marginally converted PA-M9 to PA-M8 (Fig. 13A). I collected the M8 peak and further analyzed its isomer form using an ODS-column. The M8 peak was determined to be the M8B isoform (Fig. 13B).

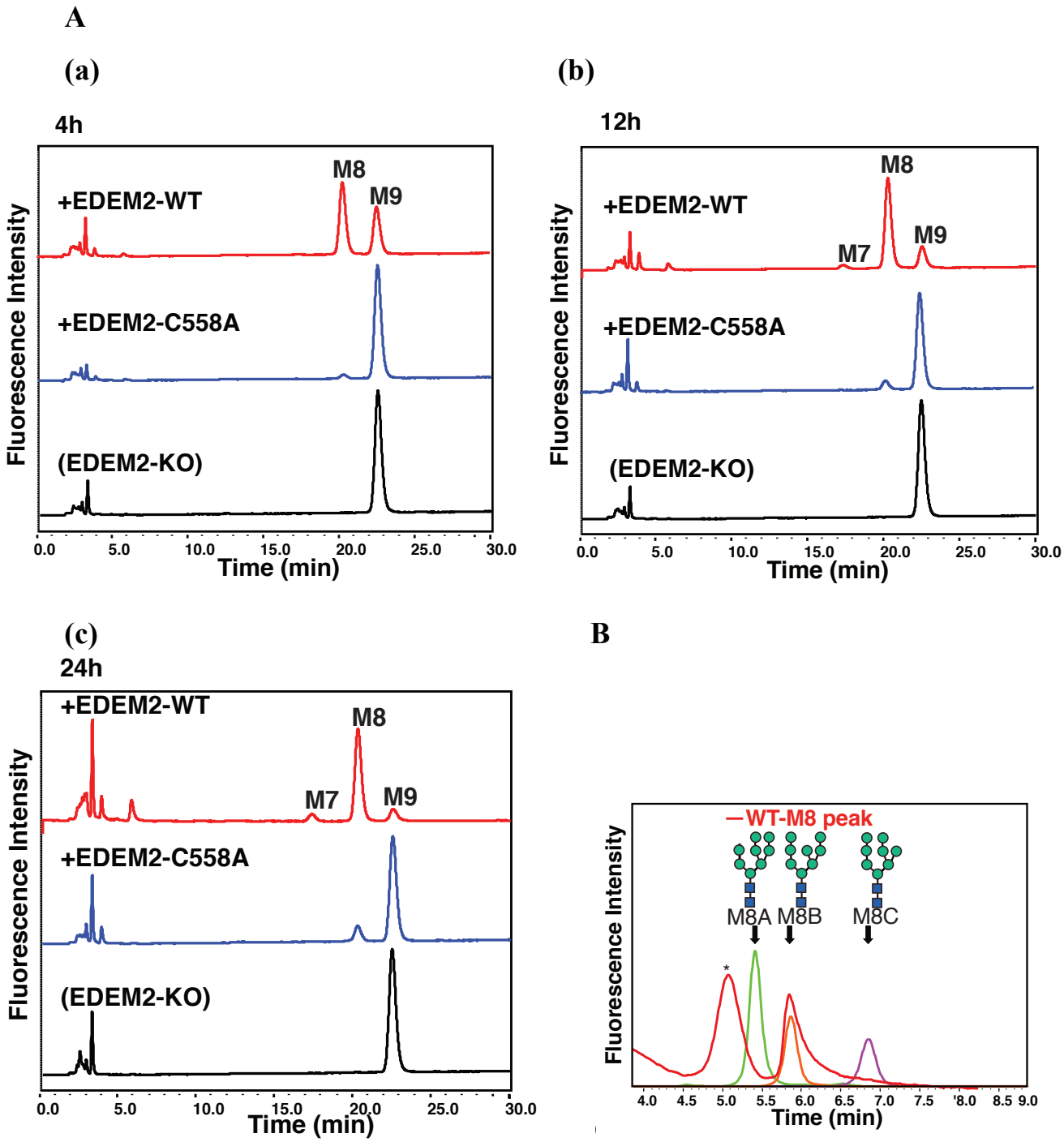

Figure 13: In vitro mannosidase activity of EDEM2-TXNDC11 complex

(A) PA-M9 was incubated with samples as indicated for 4 h **(a)**, 12 h **(b)** and 24 h **(c)**, and then analyzed by HPLC (amide column) for mannose contents. **(B)** The M8 peak obtained in (A) after incubation with WT EDEM2 was analyzed by HPLC (ODS column) for isomer identification. Green, yellow, and purple peaks indicate the elution positions of M8A, M8B, and M8C, respectively. The asterisk observed during analysis of the M8 peak denotes a fluorescent peak unrelated to oligosaccharides.

DISCUSSION

Sequential mannose trimming is critical for endoplasmic reticulum-associated degradation of misfolded glycoproteins (gpERAD). It was previously thought that trimming from M9 to M8B is conducted solely by ERmanI and that M8B is further trimmed by ERmanI or EDEM1/3 (Avezov et al., 2008; Hosokawa et al., 2010). However, gene knockout experiments in human HCT116 cells have revealed that EDEM2 is required for the first step, and EDEM3 and EDEM1 are required for the second step (Ninagawa et al., 2014). ERmanI knockout in chicken DT40 cells leads to increase in various types of B branch oligosaccharides but ERmanI knockout-cells still can proceed gpERAD. ERmanI appears to trim the outermost mannose of the B branch randomly regardless of the number of mannose residues, rather than specifically convert M9 to M8B. It was also reported that endogenous ERmanI is localized in the Golgi apparatus (Pan et al., 2011). Nonetheless, the above findings based on gene knockouts contradict the results of previous biochemical analyses. For example, it was reported that recombinant EDEM2 did not show mannosidase activity toward M9 and M8 in vitro (Mast et al., 2005). Thus, the lack of in vitro evidence of EDEM2 mannosidase activity must be solved to establish the mechanism of mammalian gpERAD.

My present study showed the vital role of the three cysteines in EDEM2 for its mannosidase activity. C65 and C408 in the MHD are strictly conserved in EDEM1, EDEM3 and yeast Htm1p (Fig 1). This evidence suggests that the architecture of the MHD in mannosidase enzymes must have been conserved in evolution from yeast to mammals. It was previously shown that, these conserved cysteines play an important role in the mannosidase activity of Htm1p (Sakoh-Nakatogawa et al., 2009). It was shown that the disulfide bond between the conserved cysteine residues, C83 and C442, in EDEM3 is mediated by ERp46 (Yu et al., 2018). ERp46 is disulfide-bonded to either C83 or C442 via its CxxC motif (Trx3) to form a high molecular weight complex (Yu et al., 2018). However, either C83S or C442S mutation eliminated the high molecular weight band, because this complex formation must be transient prior to disulfide formation between C83 and C442, which is required for mannosidase activity.

In this study, I showed that both mutations of C65 and C408 to alanine lead to defects in EDEM2 mannosidase activity and degradation of ERAD substrate CD3-δ-TM-HA (Fig 2). This suggests that C65 and C408 are likely to be linked by intramolecular disulfide bonding. As EDEM2 is associated with PDI (Fig 3A), the disulfide bond between C65 and C408 is likely to be catalyzed by PDI. However, the collision-induced dissociation (CID) mass spectrometry

(MS)/MS method of mass spectrometry analysis was not able to detect peptides in which C65 and C408 disulfide-bonded (Fig 11). The advanced mass spectrometric analysis, such as electron-transfer dissociation (ETD)/CID combined fragmentation method (Guan et al., 2018), is necessary for further confirmation of the disulfide bond formation between C65 and C408.

In EDEM2, I found that the C-terminal cysteine, C558, has an essential role in mannosidase activity and gpERAD (Fig 2B and C). EDEM2 uses this cysteine to form a stable intermolecular disulfide bond with the C692 present in the Trx5 domain of TXNDC11. The C558A mutant of EDEM2 and the C692S mutant of TXNDC11 did not rescue the defects in mannose trimming and degradation of CD3-δ-TM-HA in EDEM2-KO and TXNDC11-KO cells, respectively (Fig 2 and Fig 9).

Immunoblot showed that both EDEM2 and TXNDC11 mainly exist as a hetero dimer with each other as the monomer forms of EDEM2 and TXNDC11 are less abundant compared to their complex form (Fig 3C). Gene knockout studies of TXNDC11 clearly indicate the importance of a stable heterodimer association between TXNDC11 and EDEM2; disruption of TXNDC11 gene leads to the defect in EDEM2 mannosidase activity and degradation of gpERAD substrates such as ATF6α and CD3-δ-TM-HA is significantly delayed in TXNDC11-KO cells (Fig 6). Most importantly, this stable association with TXNDC11 is essential for EDEM2 to catalyze M9 to M8 in vitro (Fig 13). In the absence of TXNDC11, EDEM2 shows altered conformation and its degradation is enhanced, suggesting the significance of complex formation for structure of EDEM2 to express mannosidase activity (Fig 10B and C). These results demonstrate that TXNDC11 is an essential component in gpERAD and that it functions as a partner of EDEM2.

TXNDC11 is a thioredoxin-domain-containing transmembrane protein which is localized in the ER. I and Timms et al. detected TXNDC11 as a doublet band in SDS-PAGE (Timms et al., 2016). They also checked the possibility of alternative translation initiation of TXNDC11 from the M58 residue but found that M58A is still detected as a doublet band. They concluded that the doublet band may be due to partial cleavage of the signal peptide. My detailed mutational study with Endo H treatment clearly suggests that detection of TXNDC11as a doublet band is due to alternative translation initiation from the Met 58 residue (Fig 7). I therefore speculate that the doublet band found by other researchers may be due to de-glycosylation of a full length TXNDC11. I identified the significant importance of this alternative translation initiation. TXNDC11 uses alternative translation to produce membrane

and soluble versions (Fig 7). Further detailed study is necessary to clarify whether the soluble and membrane forms of TXNDC11 have distinct roles in gpERAD.

TXNDC11 contains a CxxS motif in the thioredoxin 1 domain and a CxxC motif in the thioredoxin 5 domain. Timms et al. purified the thioredoxin 5 domain and showed its reductase activity in vitro, however, they ruled out the possibility that TXNDC11 function as a reductase of ERAD substrates: the degradation of cysteine mutant of NHK (NHK C/S) is impaired similarly to wild-type NHK in TXNDC11-depleted cells. By detailed mutational analysis, I found that TXNDC11 uses C692 in the CxxC motif to stably interact with EDEM2. The mutations of other cysteines do not affect the heterodimer formation with EDEM2. Since TXNDC11 uses one of its catalytic residues to interact with C-terminal C558 of the EDEM2, it seems that the reductase function of the TXNDC11 is not applicable at least to EDEM2. Moreover, by mutation analysis I found that mutations to serine of the other cysteine residues of TXNDC11 – namely C165, C172, C380, and C574 – lead to the defect in EDEM2 mannose trimming (Fig. 8B). Perhaps these cysteine residues form intramolecular disulfide bonds with each other, which are important for TXNDC11 to function as a partner of EDEM2.

Recently, Lederkremer and collogues performed a comparative study for mannosidase activity of ERmanI, EDEM1 and EDEM2. They showed in vitro that immunoprecipitated ERmanI efficiently trimms M9 to M8, but that EDEM1 and EDEM2 have very weak trimming activities toward M8B (Shenkman et al., 2018). They also noticed that both PDI and TXNDC11 are associated with EDEM2 and EDEM1. They immunoprecipitated EDEM2 using HA antibody, from HEK293 cells expressing HA-tagged EDEM2 and Flag-tagged TXNDC11 and incubated the immunoprecipitates with denatured vitellogenin or free N-glycans released from vitellogenin but they fail to show EDEM2's mannosidase activity in vitro. They appeared to transfect HEK293 cells with HA-tagged EDEM2 cDNA (described as EDEM2-HA) and full-length TXNDC11 cDNA tagged with Flag at the N-terminus (described as Flag-TXNDC11). Accordingly, translation is initiated from the methionine located immediately upstream of the Flag-tag, resulting in detection of TXNDC11 as a single band, namely as a transmembrane protein, similarly to the M58A mutant protein. Therefore, they might not have been able to obtain sufficient amount of EDEM2-TXNDC11 complex in supernatant after lysis. In marked contrast, in the present study, I co-expressed TAP-EDEM2 and the soluble form of TXNDC11 (TXNDC11 M1A) and successfully purified a soluble complex of EDEM2-TXNDC11 which extensively trimms PA-M9 to PA-M8B.

In conclusion, the present study clearly demonstrates the mannosidase activity of EDEM2 towards free oligo saccharides in vitro, and that this effect is even clearer than the case

of yeast Htm1p. Hence, the present study represents the first clear demonstration of in vitro activity amongst EDEMs family proteins and the notion that EDEM2 catalyzes the first mannose trimming step and thereby initiates gpERAD is now firmly supported by genetic and biochemical analyses.

MATERIALS AND METHODS

Reagent type or resources	Designation	Source or reference	Identifier	Additional information
Cell line (*Homo Sapiens*)	colorectal carcinoma	ATCC	HCT116	Authenticated by ATCC and Mycoplasma tested
Recombinant DNA reagent	p3xFlag-CMV-14	Sigma-Aldrich		
Recombinant DNA reagent	pcDNA3.1-MycHis	ThermoFisher		
Antibody	anti-TXNDC11 (Rabbit monoclonal	Abcam	Cat#: ab188329	WB (1:500)
Antibody	anti-EDEM2 (Rabbit polyclonal)	Novusbio	Cat#: NBP2-37921	WB (1:500)
Antibody	anti-HA (Rabbit polyclonal)	Recenttec	Cat#: R4-TP1411100	WB (1:1000)
Antibody	anti-calnexin (Rabbit polyclonal)	Enzo Life Sciences	Cat#: ADI-SPA-865	WB (1:1000)
Antibody	anti-PDI (Rabbit polyclonal)	Enzo Life Sciences	Cat#: ADI-SPA-890	WB (1:1000)
Antibody	anti-ERp72 (Rabbit polyclonal)	Enzo Life Sciences	Cat#: ADI-SPA-720	WB (1:1000)
Antibody	anti-calreticulin (Rabbit polyclonal)	Enzo Life Sciences	Cat#: ADI-SPA-600	WB (1:1000)
Antibody	anti-Flag (Mouse monoclonal)	Sigma	Cat#: F3165	WB (1:1000) IP (2.5µl)
Antibody	anti-β-actin (Mouse monoclonal)	Wako	Cat#: 017-24573	WB (1:2000)
Antibody	Anti-human ATF6α (Rabbit polyclonal)	Haze et al., 1999		WB (1:1000)

Construction of plasmids

Recombinant DNA techniques were performed according to standard procedures (Sambrook et al., 1989) and the integrity of all constructed plasmids was confirmed by extensive sequencing analyses. Site-directed mutagenesis was carried out using mutated primers. p3xFlag-CMV-14 expression vector (Sigma) and pcDNA3.1-MycHis expression vector (ThermoFisher) were used to express a protein (EDEM2 or TXNDC11) tagged with 3xFlag and c-Myc at the C-terminus, respectively. pCMV-SP-TAP-EDEM2 was constructed based on pCMV, pcDNA3.1-SP-2xProA-2xTEV-6xMyc and pCMV-EDEM2-3xFlag using an NEBuilder HiFi DNA Assembly Cloning Kit (New England Biolabs). SP denotes a signal peptide. The ERAD-Ls substrate mCD3-δ-ΔM-HA was the kind gift of Maurizio Molinari at the Institute for Research in Biomedicine, Switzerland. pCAG-EG-TXNDC11-FP vector was constructed by inserting the target region of *TXNDC11* gene into a pCAG-EGxxFP (Addgene) vector by restriction digestion and ligation.

Cell culture, transfection and N-glycan profiling

HCT116 cells (ATCC CCL-247) were cultured in Dulbecco's modified Eagle's medium (glucose 4.5 g/liter) supplemented with 10% fetal bovine serum, 2 mM glutamine, and antibiotics (100 U/ml penicillin and 100 μg/ml streptomycin) at 37°C in a humidified 5% CO2/95% air atmosphere. Transfection was performed using mainly polyethylenimine (PEI) max (Polyscience) and partly Lipofectamine 2000 (Invitrogen) according to the manufacturers' instructions. Pyridylamination and structural identification of N-glycans of total cellular glycoproteins were performed as described previously (Horimoto et al., 2013; Ninagawa et al., 2014). EndoH was obtained from Calbiochem; cycloheximide from Sigma; MG132 from Peptide Institute; and trypsin from Nacalai Tesque. Trypsin digestion of cell lysates was carried out as described previously (Ninagawa et al., 2015).

Immunological techniques

Immunoblotting analysis was carried out according to the standard procedure (Sambrook et al., 1989) as described previously (Ninagawa et al., 2011). Chemiluminescence obtained using Western Blotting Luminol Reagent (Santa Cruz Biotechnology) was detected using a LAS-3000mini LuminoImage analyzer (Fuji Film). Rabbit monoclonal anti-TXNDC11 antibody was obtained from Abcam. Rabbit polyclonal anti-EDEM2 antibody was obtained from Novusbio; and anti-HA from Recenttec. Rabbit polyclonal anti-Calnexin, anti-PDI, and anti-ERp72 antibodies were obtained from Enzo Life Sciences. Anti-Flag antibodies were obtained from Sigma. Mouse monoclonal anti-β-actin antibody was obtained from Wako. Anti-human

ATF6 antibody was produced previously (Haze et al., 1999). Immunoprecipitation was performed using anti-Flag antibody and protein G-coupled Sepharose beads (GE Healthcare). Beads were washed with high salt buffer (50 mM Tris/Cl, pH 8.0, containing 1% NP-40 and 150 mM NaCl) twice, washed with PBS, and boiled in Laemmli's sample buffer.

CRISPR/Cas9-based PITCh system

TXNDC11 gene knockout was done as previously described (Sakuma et al., 2016). Briefly, the oligonucleotides 5'-caccGCAGCGCGCAGCCGAGCGCCA-3' and 5'-aaacTGGCGCTCGGCTGCGCGCTGC-3' to express gRNA for cleavage of exon 1 of the *TXNDC11* gene (lower case letters denote cohesive ends for ligation) were annealed and inserted into the BpiI site of pX330A-1x2 (Addgene). The BsaI fragment of pX330S-2-PITCh to express PITCh gRNA (Addgene) was inserted into the resulting vector to create pX330A-TXNDC11-PITCh1x2 (Fig. 3A). The 5' forward primer 5'-ccgcgttacatagcatcgtacgcgtacgtgtttggAGCTGCTCTGCGGGGCCGTG-ccggatccggcccgctagcacgtattta-3' corresponding to the PITCh gRNA target site (5'-side lower case letters), the left arm of the *TXNDC11* gene (upper case letters) and the vector sequence (3'-side lower case letters), as well as the 3' reverse primer 5'-acgcgtacgtgtttggAGGAGCAGCGCGCAGCCGAGcgcgccttaagtcgacaag-3' corresponding to the PITCh gRNA target site (5'-side lower case letters), the right arm of the *TXNDC11* gene (upper case letters) and the vector sequence (3'-side lower case letters) were used to amplify the region containing the puromycin-resistant gene but not the EGFP gene in pCRIS-PITChv2-FBL followed by infusion reaction to create pCRIS-Puro (Fig. 3A). HCT116 cells were transfected with pX330A-TXNDC11-PITCh1x2 and pCRIS-Puro using PEI-max and screened for puromycin resistance.

Genomic PCR

Homologous recombination in HCT116 cells was confirmed by genomic PCR using a pair of primers 753Fw: 5'-CTACAGCGGTGTCAAGGTTCCAAGTAT-3' and 1708Rv: 5'-AAGTGACAGGTCCACCCCTAGTGACTC-3', 730Fw: 5'-AGACTACAGCGGTGTCAAGGTTCCAAGTAT-3' and 1831Rv: 5'-TTAGATCAATGAGTGCGGGAATTCTAAAAG-3', and TgFw: 5'-AGTATGACAGGAAAAACTTCCATTTTAGTG-3' and TgRv: 5'-TATTAGGTCTGAAGAGGAGTTTACGTCCAG-3'.

RT-PCR

Total RNA prepared from cultured cells (~5 × 10^6 cells) by the acid guanidinium/phenol/chloroform method using ISOGEN (Nippon Gene) was converted to cDNA using Moloney murine leukemia virus reverse transcription (Invitrogen) and random primers. The full-length open reading frame of TXNDC11 and GAPDH was amplified using PrimeSTAR HS DNA polymerase (Takara Bio) and a pair of primers, 5′-GGAATTCGGTCGGAATGCGGAGGCCGCGGC-3′ and 5′-TCGGTCGACTTAGTCTGTCCTGTTCTCCTT-3′, for TXNDC11 and 5'-ATTCCATGGCACCGTCAAG-3' and 5'-GATCTCGCTCCTGGAAGATG-3' for GAPDH, respectively.

Quantitative RT-PCR

Total RNA extracted as above was subjected to quantitative RT-PCR analysis using the SYBR Green method (Applied Biosystems) and a pair of primers, namely 778Fw: 5'-GGAGAGCCGGTCAGATATCG-3' and 838Rv: 5'-CCACTTGCCAGTGAGCACAT-3' as well as 1036Fw: 5'-CCAGTCCTTGGAGGCCTACTG-3' and 1105Rv: 5'-GGTCCTCATGGCATTGTCAAT-3' for *EDEM2* mRNA, Fw: 5'-CTGCTGAGTCCGCATCAGGT-3' and Rv: 5'-GAGTCAATACCGCCAGAATCCA-3' for spliced *XBP1* mRNA, and Fw: 5'-ATTCCATGGCACCGTCAAG-3' and Rv: 5'-GATCTCGCTCCTGGAAGATG-3' for *GAPDH* mRNA.

Repeated freezing and thawing

TXNDC11-KO cells in 10-cm dishes were collected 16 h after transfection in 1 ml of PBS containing protease inhibitor cocktail and MG132, and centrifuged at 5,000 rpm for 3 min. The pellets were re-suspended in 600 μl of PBS containing protease inhibitor cocktail and MG132, quickly frozen in liquid nitrogen, and then quickly thawed in a water bath at 37°C. This freezing and thawing cycle was repeated 10 times. After centrifugation at 1,000 x g for 10 min, the supernatant was collected, subjected to further 5 cycles of freezing and thawing, and centrifuged at 1,000 x g for 10 min. Half of the supernatant was used as total membrane fraction (T). The second half of the supernatant was centrifuged at 40,000 rpm for 30 min at 4°C to collect supernatant (S) and pellets (P).

DNA-Maleimide modification assay

Modification of cysteines in EDEM2 was performed using a protein redox state monitoring kit according to the manufacturer's protocol (SulfoBiotics) (Hara et al., 2013). Briefly, NEM treated with lysates from WT, TXNDC11-KO and EDEM2-KO cells were TCA-precipitated

and then washed with acetone. The samples were dried and then solubilized using a sonicator. The soluble samples were further treated with DTT to reduce the disulfide bonded cysteines, followed by TCA precipitation, washing, and sonication as described before. From the final solubilized samples, 4 µl was used for DNA-maleimide modification. Initially, 4 µl of reaction buffer A was added to protein-shifter. Then, 4 µl of sample was mixed with the above reaction by pipetting. Finally, 4 µl of reaction buffer B was added to the solution and mixed properly. The reaction was incubated at 37°C for 30 min. The incubated samples were electrophoresed with reducing SDS-PAGE and the gel were incubated under UV for 15 min to remove the DNA-tag prior to western blot.

Purification of EDEM2

EDEM2-KO cells plated on 15 cm dishes were simultaneously transfected with TAP-EDEM2 and TXNDC11(M1A)-3xFlag. Forty-eight hours later the cells were lysed in lysis buffer {50 mM MES, pH 7.5, containing 150 mM NaCl, 1% CHAPS, and EDTA-free protease inhibitor cocktail (Roche)}, and centrifuged at 9,500 g for 30 min at 4°C. The resulting supernatant was filtrated through a low protein binding syringe filter (Merck) and rotated for 8 h at 4°C after the addition of IgG Sepharose beads (GE Health Care). The beads were collected by centrifugation at 3,000 rpm for 1 min at 4°C, washed twice briefly and then washed overnight with wash buffer (50 mM MES, pH7.5, containing 400 mM NaCl, 0.1% CHAPS and EDTA-free protease inhibitor cocktail). The beads were incubated with 200 U of AcTEV protease (Invitrogen) in TEV buffer (50 mM MES, pH7.5, containing 150 mM NaCl) for 24 h at 4ºC, and then centrifuged briefly. The resulting supernatant was concentrated using an Amicon Filter (10 kDa cut off, Millipore) by centrifugation at 4,000 g for 1h at 4°C. During concentration the buffer was changed to 50 mM MES, pH7.5, containing 150 mM NaCl and 5 mM $CaCl_2$, by 3 additions to the filter.

Sample processing for proteome analysis

In-gel digestion was performed according to a protocol (Shevchenko et al., 2006). Briefly, gel pieces (IAA-treated) were dehydrated with 500 µl of 100% ACN and incubated at room temperature for 15 min, after which the ACN was discarded. The remaining ACN solution was evaporated under reduced pressure using a SpeedVac. Proteins were digested with trypsin (Promega) (1.7 µg) in 50 mM ABC (ammonium bicarbonate) and incubated for 30 min on ice, followed by additional incubation at room temperature for 90 min. 100 ul of 50 mM ABC was added to each sample, and the samples were incubated at 37°C for 16 h. Next day, 100 µl of AspN (1.7 µg) in 50 mM ABC was added to each sample and incubated at 37°C for 3 h. The

peptides were transferred to a fresh tube. Peptides were extracted from the gels using 150 µl of 3% TFA, 30% ACN (incubated for 5 min with gentle shaking), followed by 200 µl of ACN (incubated for 5 min with gentle shaking). The extracted peptides were transferred to a corresponding fresh tube, and the sample solution was evaporated using SpeedVac at 55°C for 1.5 h. Peptides were desalted with SDB-XC StageTips prior to LC/MS/MS analysis (Rappsilber et al., 2007).

Mass Spectrometric analysis

Nano-scale reversed-phase liquid chromatography coupled with tandem mass spectrometry (nanoLC/MS/MS) was performed with an Orbitrap Fusion Lumos mass spectrometer (Thermo Fisher Scientific), connected to a Thermo Ultimate 3000 RSLCnano pump and an HTC-PAL autosampler (CTC Analytics) equipped with a self-pulled analytical column (150 mm length × 100 µm i.d.) (Ishihama et al., 2002) packed with ReproSil-Pur C18-AQ materials (3 µm, Dr. Maisch GMBH). The mobile phases consisted of (A) 0.5% acetic acid and (B) 0.5% acetic acid and 80% acetonitrile. Peptides were eluted from the analytical column at a flow rate of 500 nl/min by altering the gradient: 5-10% B in 5 min, 10-40% B in 15 min, 40-100% B in 1 min and 100% for 4 min. The Orbitrap Fusion Lumos instrument was operated in data-dependent mode with a full scan in the Orbitrap followed by MS/MS scans for 3 sec using higher-energy collision dissociation (HCD). The applied voltage for ionization was 2.4 kV. The full scans were performed with a resolution of 120,000, a target value of $4x10^5$ ions and a maximum injection time of 50 ms. The MS scan range was *m/z* 300–1,500. The MS/MS scans were performed with a 15,000 resolution, a $5x10^4$ target value and a 50 ms maximum injection time. The isolation window was set to 1.6 and normalized HCD collision energy was 30. Dynamic exclusion was applied for 20 sec.

All raw datasets were analyzed and processed by MaxQuant (v1.6.5.0) (Cox J et al., 2008). Default settings were employed. Search parameters included two missed cleavage sites and variable modifications such as methionine oxidation, protein N-terminal acetylation and cysteine carbamidomethyl. The peptide mass tolerance was 6 ppm and the MS/MS tolerance were 20 ppm. The database search was performed with Andromeda (Cox et al., 2011) against the UniProt human database (downloaded on 2019-4) with common contaminants and enzyme sequences. False discovery rate (FDR) was set to 1% at the peptide spectrum match (PSM) level and at the protein level. For protein quantification, the total summed intensity of the peptides was used. A minimum peptide count required for protein quantification was set to two.

In vitro mannosidase assay

PA-labeled free oligosaccharides were purchased from Takara Bio. Approximately 90 ng of purified WT and C558A mutant of EDEM2 were incubated with 50 μM PA-M9 in a total volume of 45 μl of assay buffer (50 mM MES, pH 7.5, containing 150 mM NaCl and 5 mM $CaCl_2$) for 4 h, 12 h, or 24 h at 37ºC. The reaction was stopped by boiling for 5 min. The samples were evaporated, dissolved with 20 μl of 70% (v/v) acetonitrile, and analyzed using a TSK-gel Amide-80 column (Tosoh) for mannose contents. Identification of *N*-glycan structures was based on their elution positions on the column and their molecular mass values compared with those of PA-glycans in the GALAXY database (http://www.glycoanalysis.info/galaxy2/ENG/index.jsp) (Takahashi et al., 2003). The M8 peak from the WT sample was collected, evaporated, dissolved with 20 μl of water, and analyzed using a Shim-pack HRC-octadecyl silica column (Shimadzu) for isomer identification.

ACKNOWLDGEMENTS

I sent an email to Prof. Kazutoshi Mori in 2014 regarding my interest in doing a PhD under his supervision. Fortunately, he responded that I should apply for an MEXT scholarship. I applied for the scholarship, but with my bad luck did not pass the second round of screening. I again mailed him about my situation. He told me to meet him at a conference in India. He interviewed me there and agreed to apply for MEXT scholarship under Kyoto University recommendation. Again, the hurdle arose that score I received for my master's degree did not meet the eligibility criteria for a Kyoto university recommendation. Finally, with all hope lost, Prof. Mori advised me to give up my plan. I had followed this plan for around 2 years so of course the situation left me feeling helpless. But I held on to my goal and replied to him that I would come to Japan without a scholarship. There were many reasons for me to give up my plan, but I considered only one reason in rejecting them all, namely my interest to do research under Prof. Mori. Before coming to Japan, I was prepared for the possibility that I may not complete my degree due to my financial condition, but I thought at least I will try to survive as much as I can. I believe one thing about nature's rule: if you decide to do something from heart, all barriers and hurdles will eventually melt away. I could not have completed this PhD without the support of my supervisor, Prof. Mori. He supported me substantially throughout the 3 years of my stay, both financially and in guiding my research in the right direction. He decided to give lab presentations in both English and Japanese to overcome the language barrier –my inability to speak Japanese well– a barrier to which almost all other foreign students are subject. He also took initiative in obtaining a scholarship for me, and finally I succeed to obtaining one. I feel very strong gratitude to Mori-sensei for his sincere support, which is beyond words. I am so lucky to have done my doctoral degree under a renowned scientist like Mori Sensei. I am always proud of Mori-sensei for his breakthrough discoveries in UPR and his prestigious awards. I suspect that I am the most frequent visitor to his Wikipedia page and online motivational videos. He inspired me a lot with his dedicated research career.

Second, I am very grateful to Dr. Tetsuya Okada. From the first day of my life in Japan he came to greet me, and supported me throughout. I was very new to molecular biology techniques. He taught me from the very beginning with great patience and helped me develop expertise in almost all the experiments which I performed for this work. He also strongly helped me in obtaining scholarships, and supported me morally throughout my study. I still remember when he came to inform me that I had won the scholarship - he was more excited and happier than me. I was very fortunate in getting such a great teacher as Okada-sensei. I did

not feel any barrier in talking with him freely. Whenever I became stuck in any experiment, the first name which came to mind for help was Okada-sensei, and I ran towards his desk for advice.

I am grateful to my talented and dedicated lab senior, Ninagawa-san, who identified the role of EDEM2 in his previous studies. He performed the degradation assays in my present research and also advised me in experiments. He also supported me when I face a financial crisis. Beyond the lab works, I enjoyed marathon running and other party events with him. I also wanted to thank Ishikawa-sensei for guiding me with plasmid construction. He always encouraged me to discuss the progress of my work and gave good suggestions about my research.

I was fortunate to have Jin-san, Ikeda-san, Koba-san, Yasuda-kun and Kin kun as my lab colleagues. They guided and helped me during my first days in Japan and also helped me to write my scholarship application. I consider Jin-san to be a good friend for sharing his knowledge whenever I was stuck with anything. I would like to also thank all the other Mori lab members for making my stay comfortable and lively.

I also wanted to thank our dedicated lab secretary Miyagawa-san for her timely support of administrative work and lab ordering, and also administrative officer Imanishi-san for her great support regarding official procedures.

I am very happy to have had good collaboration with Yagi-sensei during the in vitro mannosidase analysis. He guided me a lot regarding the use of HPLC. I also want to thank Imami-sensei for his collaborative work in mass spectrometry analysis.

I am indebted to the T Banaji Scholarship Foundation, which provided me with a scholarship for two years.

I am very thankful to my family for their support, especially my mother and sister. My mother has always encouraged me to reach for higher studies.

Apart from a research-oriented life, I was blessed with having a great social life at Kyoto University. I am grateful to my two close friends, Monika and Adi, for their moral support. My personal life in Japan always revolved around them. I enjoyed trips and cooking with them, which gave me a positive outlook. I also want to extend my thanks to my many other friends - too numerous to list - for their company, especially Partha, Chanchal, Sudhanshu, Harshal, Chinmoy, and Sandeep Goel, Nikunj, Sudeepa, Nitin, Mansoor, among others.

PUBLICATIONS

Ginto George, Satoshi Ninagawa, Hirokazu Yagi, Taiki Saito, Tokiro Ishikawa, Tetsushi Sakuma, Takashi Yamamoto, Koshi Imami, Yasushi Ishihama, Koichi Kato, Tetsuya Okada, and Kazutoshi Mori.
EDEM2 Stably Disulfide-bonded to TXNDC11 Catalyzes the First Mannose Trimming Step in Mammalian Glycoprotein ERAD.
eLife 2020;9:e53455 (2020). DOI: 10.7554/eLife.53455

REFERENCES

Avezov, E., Z. Frenkel, M. Ehrlich, A. Herscovics and G. Z. Lederkremer (2008). "Endoplasmic reticulum (ER) mannosidase I is compartmentalized and required for N-glycan trimming to Man5-6GlcNAc2 in glycoprotein ER-associated degradation." Mol Biol Cell 19(1): 216-225.

Bernasconi, R., C. Galli, V. Calanca, T. Nakajima and M. Molinari (2010). "Stringent requirement for HRD1, SEL1L, and OS-9/XTP3-B for disposal of ERAD-LS substrates." J Cell Biol 188(2): 223-235.

Brodsky, J. L. (2012). "Cleaning up: ER-associated degradation to the rescue." Cell 151(6): 1163-1167.

Clavel, C., G. Chavanel and P. Birembaut (1986). "Detection of the plasmin system in human mammary pathology using immunofluorescence." Cancer Res 46(11): 5743-5747.

Clerc, S., C. Hirsch, D. M. Oggier, P. Deprez, C. Jakob, T. Sommer and M. Aebi (2009). "Htm1 protein generates the N-glycan signal for glycoprotein degradation in the endoplasmic reticulum." J Cell Biol 184(1): 159-172.

Cox, J. and M. Mann (2008). "MaxQuant enables high peptide identification rates, individualized p.p.b.-range mass accuracies and proteome-wide protein quantification." Nat Biotechnol 26(12): 1367-1372.

Cox, J., N. Neuhauser, A. Michalski, R. A. Scheltema, J. V. Olsen and M. Mann (2011). "Andromeda: a peptide search engine integrated into the MaxQuant environment." J Proteome Res 10(4): 1794-1805.

Gauss, R., K. Kanehara, P. Carvalho, D. T. Ng and M. Aebi (2011). "A complex of Pdi1p and the mannosidase Htm1p initiates clearance of unfolded glycoproteins from the endoplasmic reticulum." Mol Cell 42(6): 782-793.

Gonzalez, D. S., K. Karaveg, A. S. Vandersall-Nairn, A. Lal and K. W. Moremen (1999). "Identification, expression, and characterization of a cDNA encoding human endoplasmic reticulum mannosidase I, the enzyme that catalyzes the first mannose trimming step in mammalian Asn-linked oligosaccharide biosynthesis." J Biol Chem 274(30): 21375-21386.

Guan, X., L. Zhang and J. Wypych (2018). "Direct mass spectrometric characterization of disulfide linkages." MAbs 10(4): 572-582.

Hammond, C., I. Braakman and A. Helenius (1994). "Role of N-linked oligosaccharide recognition, glucose trimming, and calnexin in glycoprotein folding and quality control." Proc Natl Acad Sci U S A 91(3): 913-917.

Hara, S., T. Nojima, K. Seio, M. Yoshida and T. Hisabori (2013). "DNA-maleimide: an improved maleimide compound for electrophoresis-based titration of reactive thiols in a specific protein." Biochim Biophys Acta 1830(4): 3077-3081.

Haze, K., H. Yoshida, H. Yanagi, T. Yura and K. Mori (1999). "Mammalian transcription factor ATF6 is synthesized as a transmembrane protein and activated by proteolysis in response to endoplasmic reticulum stress." Mol Biol Cell 10(11): 3787-3799.

Hebert, D. N., B. Foellmer and A. Helenius (1995). "Glucose trimming and reglucosylation determine glycoprotein association with calnexin in the endoplasmic reticulum." Cell 81(3): 425-433.

Hirao, K., Y. Natsuka, T. Tamura, I. Wada, D. Morito, S. Natsuka, P. Romero, B. Sleno, L. O. Tremblay, A. Herscovics, K. Nagata and N. Hosokawa (2006). "EDEM3, a soluble EDEM homolog, enhances glycoprotein endoplasmic reticulum-associated degradation and mannose trimming." J Biol Chem 281(14): 9650-9658.

Horimoto, S., S. Ninagawa, T. Okada, H. Koba, T. Sugimoto, Y. Kamiya, K. Kato, S. Takeda and K. Mori (2013). "The unfolded protein response transducer ATF6 represents a novel transmembrane-type endoplasmic reticulum-associated degradation substrate requiring both mannose trimming and SEL1L protein." J Biol Chem 288(44): 31517-31527.

Hosokawa, N., Y. Kamiya and K. Kato (2010). "The role of MRH domain-containing lectins in ERAD." Glycobiology 20(6): 651-660.

Hosokawa, N., L. O. Tremblay, B. Sleno, Y. Kamiya, I. Wada, K. Nagata, K. Kato and A. Herscovics (2010). "EDEM1 accelerates the trimming of alpha1,2-linked mannose on the C branch of N-glycans." Glycobiology 20(5): 567-575.

Hosokawa, N., L. O. Tremblay, B. Sleno, Y. Kamiya, I. Wada, K. Nagata, K. Kato and A. Herscovics (2010). "EDEM1 accelerates the trimming of alpha1,2-linked mannose on the C branch of N-glycans." Glycobiology 20(5): 567-575.

Hosokawa, N., L. O. Tremblay, Z. You, A. Herscovics, I. Wada and K. Nagata (2003). "Enhancement of endoplasmic reticulum (ER) degradation of misfolded Null Hong Kong alpha1-antitrypsin by human ER mannosidase I." J Biol Chem 278(28): 26287-26294.

Ishihama, Y., J. Rappsilber, J. S. Andersen and M. Mann (2002). "Microcolumns with self-assembled particle frits for proteomics." J Chromatogr A 979(1-2): 233-239.

Kamiya, Y., T. Satoh and K. Kato (2012). "Molecular and structural basis for N-glycan-dependent determination of glycoprotein fates in cells." Biochim Biophys Acta 1820(9): 1327-1337.

Kojima, R., M. Okumura, S. Masui, S. Kanemura, M. Inoue, M. Saiki, H. Yamaguchi, T. Hikima, M. Suzuki, S. Akiyama and K. Inaba (2014). "Radically different thioredoxin domain arrangement of ERp46, an efficient disulfide bond introducer of the mammalian PDI family." Structure 22(3): 431-443.

Mast, S. W., K. Diekman, K. Karaveg, A. Davis, R. N. Sifers and K. W. Moremen (2005). "Human EDEM2, a novel homolog of family 47 glycosidases, is involved in ER-associated degradation of glycoproteins." Glycobiology 15(4): 421-436.

Molinari, M. (2007). "N-glycan structure dictates extension of protein folding or onset of disposal." Nat Chem Biol 3(6): 313-320.

Ninagawa, S., T. Okada, Y. Sumitomo, S. Horimoto, T. Sugimoto, T. Ishikawa, S. Takeda, T. Yamamoto, T. Suzuki, Y. Kamiya, K. Kato and K. Mori (2015). "Forcible destruction of severely misfolded mammalian glycoproteins by the non-glycoprotein ERAD pathway." J Cell Biol 211(4): 775-784.

Ninagawa, S., T. Okada, Y. Sumitomo, Y. Kamiya, K. Kato, S. Horimoto, T. Ishikawa, S. Takeda, T. Sakuma, T. Yamamoto and K. Mori (2014). "EDEM2 initiates mammalian glycoprotein ERAD by catalyzing the first mannose trimming step." J Cell Biol 206(3): 347-356.

.

Ninagawa, S., T. Okada, S. Takeda and K. Mori (2011). "SEL1L is required for endoplasmic reticulum-associated degradation of misfolded luminal proteins but not transmembrane proteins in chicken DT40 cell line." Cell Struct Funct 36(2): 187-195.

Olivari, S., T. Cali, K. E. Salo, P. Paganetti, L. W. Ruddock and M. Molinari (2006). "EDEM1 regulates ER-associated degradation by accelerating de-mannosylation of folding-defective polypeptides and by inhibiting their covalent aggregation." Biochem Biophys Res Commun 349(4): 1278-1284.

Pan, S., S. Wang, B. Utama, L. Huang, N. Blok, M. K. Estes, K. W. Moremen and R. N. Sifers (2011). "Golgi localization of ERManI defines spatial separation of the mammalian glycoprotein quality control system." Mol Biol Cell 22(16): 2810-2822.

Quan, E. M., Y. Kamiya, D. Kamiya, V. Denic, J. Weibezahn, K. Kato and J. S. Weissman (2008). "Defining the glycan destruction signal for endoplasmic reticulum-associated degradation." Mol Cell 32(6): 870-877.

Rappsilber, J., M. Mann and Y. Ishihama (2007). "Protocol for micro-purification, enrichment, pre-fractionation and storage of peptides for proteomics using StageTips." Nat Protoc 2(8): 1896-1906.

Roschke, A. V., K. Stover, G. Tonon, A. A. Schaffer and I. R. Kirsch (2002). "Stable karyotypes in epithelial cancer cell lines despite high rates of ongoing structural and numerical chromosomal instability." Neoplasia 4(1): 19-31.

Sakoh-Nakatogawa, M., S. Nishikawa and T. Endo (2009). "Roles of protein-disulfide isomerase-mediated disulfide bond formation of yeast Mnl1p in endoplasmic reticulum-associated degradation." J Biol Chem 284(18): 11815-11825.

Sakuma, T., S. Nakade, Y. Sakane, K. T. Suzuki and T. Yamamoto (2016). "MMEJ-assisted gene knock-in using TALENs and CRISPR-Cas9 with the PITCh systems." Nat Protoc 11(1): 118-133.

Sambrook, J., E.F. Fritsch, and T. Maniatis. 1989. Molecular Cloning: A Laboratory Manual. Cold Spring Harbor Laboratory Press, Cold Spring Harbor, New York.

Shenkman, M., E. Ron, R. Yehuda, R. Benyair, I. Khalaila and G. Z. Lederkremer (2018). "Mannosidase activity of EDEM1 and EDEM2 depends on an unfolded state of their glycoprotein substrates." Commun Biol 1: 172.

Shevchenko, A., H. Tomas, J. Havlis, J. V. Olsen and M. Mann (2006). "In-gel digestion for mass spectrometric characterization of proteins and proteomes." Nat Protoc 1(6): 2856-2860.

Smith, M. H., H. L. Ploegh and J. S. Weissman (2011). "Road to ruin: targeting proteins for degradation in the endoplasmic reticulum." Science 334(6059): 1086-1090.

Spiro, R. G., Q. Zhu, V. Bhoyroo and H. D. Soling (1996). "Definition of the lectin-like properties of the molecular chaperone, calreticulin, and demonstration of its copurification with endomannosidase from rat liver Golgi." J Biol Chem 271(19): 11588-11594.

Sun, Z. and J. L. Brodsky (2019). "Protein quality control in the secretory pathway." J Cell Biol 218(10): 3171-3187.

Takahashi, N., and K. Kato. 2003. GALAXY (Glycoanalysis by the Three Axes of MS and Chromatography): a Web Application that Assists Structural Analyses of N-Glycans. *Trends Glycosci. Glycotech.* 15:235-251.

Timms, R. T., S. A. Menzies, I. A. Tchasovnikarova, L. C. Christensen, J. C. Williamson, R. Antrobus, G. Dougan, L. Ellgaard and P. J. Lehner (2016). "Genetic dissection of mammalian ERAD through comparative haploid and CRISPR forward genetic screens." Nat Commun 7: 11786.

Tsai, B., Y. Ye and T. A. Rapoport (2002). "Retro-translocation of proteins from the endoplasmic reticulum into the cytosol." Nat Rev Mol Cell Biol 3(4): 246-255.

van der Goot, A. T., M. M. P. Pearce, D. E. Leto, T. A. Shaler and R. R. Kopito (2018). "Redundant and Antagonistic Roles of XTP3B and OS9 in Decoding Glycan and Non-glycan Degrons in ER-Associated Degradation." Mol Cell 70(3): 516-530 e516.

Ware, F. E., A. Vassilakos, P. A. Peterson, M. R. Jackson, M. A. Lehrman and D. B. Williams (1995). "The molecular chaperone calnexin binds $Glc_1Man_9GlcNAc_2$ oligosaccharide as an initial step in recognizing unfolded glycoproteins." J Biol Chem 270(9): 4697-4704.

Xie, W. and D. T. Ng (2010). "ERAD substrate recognition in budding yeast." Semin Cell Dev Biol 21(5): 533-539.

Yu, S., S. Ito, I. Wada and N. Hosokawa (2018). "ER-resident protein 46 (ERp46) triggers the mannose-trimming activity of ER degradation-enhancing alpha-mannosidase-like protein 3 (EDEM3)." J Biol Chem 293(27): 10663-10674.